Key Points:
- Asymmetric amplification of surface ocean pCO_2 and pH seasonal cycles is anticipated over the 21st century under RCP8.5
- Expected seasonal asymmetries highlight ongoing challenges with using a summer-biased observing network to estimate anthropogenic trends
- Projecting onto Revelle factor perturbations, the pCO_2 seasonal cycle response may have important implications for carbon cycle feedbacks

Seasonal Asymmetry in the Evolution of Surface Ocean pCO_2 and pH Thermodynamic Drivers and the Influence on Sea-Air CO_2 Flux

Andrea J. Fassbender[1] , Keith B. Rodgers[2,3] , Hilary I. Palevsky[4,5] , and Christopher L. Sabine[6,7]

[1]Monterey Bay Aquarium Research Institute, Moss Landing, CA, USA, [2]Center for Climate Physics, Institute for Basic Science, Busan, South Korea, [3]Pusan National University, Busan, South Korea, [4]Department of Marine Chemistry and Geochemistry, Woods Hole Oceanographic Institution, Falmouth, MA, USA, [5]Now at the Department of Geosciences, Wellesley College, Wellesley, MA, USA, [6]Pacific Marine Environmental Laboratory, National Oceanic and Atmospheric Administration, Seattle, WA, USA, [7]Now at the Department of Oceanography, SOEST, University of Hawai'i at Mānoa, Honolulu, HI, USA

Abstract It has become clear that anthropogenic carbon invasion into the surface ocean drives changes in the seasonal cycles of carbon dioxide partial pressure (pCO_2) and pH. However, it is not yet known whether the resulting sea-air CO_2 fluxes are symmetric in their seasonal expression. Here we consider a novel application of observational constraints and modeling inferences to test the hypothesis that changes in the ocean's Revelle factor facilitate a seasonally asymmetric response in pCO_2 and the sea-air CO_2 flux. We use an analytical framework that builds on observed sea surface pCO_2 variability for the modern era and incorporates transient dissolved inorganic carbon concentrations from an Earth system model. Our findings reveal asymmetric amplification of pCO_2 and pH seasonal cycles by a factor of two (or more) above preindustrial levels under Representative Concentration Pathway 8.5. These changes are significantly larger than observed modes of interannual variability and are relevant to climate feedbacks associated with Revelle factor perturbations. Notably, this response occurs in the absence of changes to the seasonal cycle amplitudes of dissolved inorganic carbon, total alkalinity, salinity, and temperature, indicating that significant alteration of surface pCO_2 can occur without modifying the physical or biological ocean state. This result challenges the historical paradigm that if the same amount of carbon and nutrients is entrained and subsequently exported, there is no impact on anthropogenic carbon uptake. Anticipation of seasonal asymmetries in the sea surface pCO_2 and CO_2 flux response to ocean carbon uptake over the 21st century may have important implications for carbon cycle feedbacks.

Plain Language Summary The ocean uptake of human released carbon dioxide (CO_2) is causing the natural seasonal swings in seawater CO_2 to grow over time. Using observations and numerical models, we conduct a theoretical experiment to see how the surface ocean may respond to continued carbon additions under "business-as-usual" future atmospheric CO_2 concentrations. We find that between 1861 and 2100, the chemical properties of CO_2 in seawater cause the seasonal CO_2 maximum to grow by more than the seasonal CO_2 minimum. As a result, the rate of summer surface ocean CO_2 growth is different than winter, requiring year-round observations to accurately measure the overall annual ocean carbon absorption. Additionally, these seasonal CO_2 changes affect how much carbon is lost from the ocean during high-CO_2 periods relative to how much carbon is gained from the atmosphere during low-CO_2 periods, creating a trend in the average ocean carbon absorption over years to decades that must be considered in the interpretation of marine carbon cycle observations and numerical models. These findings are important as they have implications for future rates of climate change and ocean acidification.

1. Introduction

A significant body of scientific literature has focused on understanding modern rates of change in sea surface carbonate chemistry to better characterize how the ocean is responding to rising atmospheric carbon dioxide (CO_2) levels (Fay & McKinley, 2013; Landschützer et al., 2016; Lauvset et al., 2015; Lovenduski et al., 2015; McKinley et al., 2017). Some of the most compelling observational data come from well-maintained time series sites where more than a decade of observations have been evaluated (Bates et al., 2014; González-Dávila et al., 2010; Munro et al., 2015; Olafsson et al., 2009; Sutton et al., 2014; Takahashi et al., 2009, 2014).

Still, separating anthropogenic forcing from natural variability in the partial pressure of CO_2 (pCO_2) remains a fundamental challenge (Ilyina, 2016; McKinley et al., 2016), as natural and secular changes in other seawater parameters (such as salinity or temperature) also influence the sea surface carbonate chemistry (Takahashi et al., 1993). Our understanding of these compounding processes continues to improve thanks to the many researchers who investigate observed (Hagens & Middelburg, 2016; Landschützer et al., 2014; Lenton et al., 2012; Thomas et al., 2007) and simulated (Lovenduski et al., 2015; McKinley et al., 2006) variability in ocean carbonate chemistry, quantify the modern global sea-air CO_2 flux (Landschützer et al., 2016; Takahashi et al., 2009; Wanninkhof et al., 2013), and use models to interpret ocean chemistry changes related to carbon uptake and storage (Arora et al., 2013; Friedlingstein et al., 2003; Friedlingstein et al., 2006; Gregory et al., 2009; Hauck et al., 2015; Hauck & Völker, 2015; Le Quéré et al., 2015, 2016, 2018; Schwinger et al., 2014).

In particular, concerted modeling and data analysis efforts have been devoted to understanding the relationship between climate modes of variability (e.g., Southern Annular Mode, El Niño Southern Oscillation, and North Atlantic Oscillation) and their associated perturbations to regional sea-air CO_2 fluxes. For the case of the Southern Ocean and Southern Annular Mode, this was originally addressed by Lenton and Matear (2007), Lovenduski et al. (2007), and Le Quéré et al. (2007). An underlying assumption in these approaches has been that the seasonal pCO_2 cycle is stationary, and anomalies relative to the static seasonal cycle can be used to address climate variability responses. Through this lens, it is expected that interannual modes of climate variability can serve as emergent constraints (Hall & Qu, 2006; Kwiatkowski et al., 2017) for future climate change. In other words, the relationship between CO_2 flux variations and contemporary modes of climate variability is assumed to have direct pertinence to the sensitivity of CO_2 fluxes to secular, anthropogenic climate change. Therefore, inherent to this methodology is the hypothesis that the processes maintaining the seasonal cycle are independent of the processes maintaining the secular trend in the ocean carbon cycle state.

However, in the past decade, several independent modeling studies have determined that the seasonal cycle of carbon variables in the surface ocean is not expected to be stationary, but rather to exhibit an increasing (and for some parameters decreasing) seasonal amplitude associated with the invasion of anthropogenic CO_2 (Gorgues et al., 2010; Hauck et al., 2015; Hauck & Völker, 2015; Kwiatkowski & Orr, 2018; McNeil & Sasse, 2016; Pacella et al., 2018; Riebesell et al., 2009; Rodgers et al., 2008; Sasse et al., 2015). Very recently, observation-based evidence of pCO_2 seasonal cycle amplification across broad ocean realms was presented by Landschützer et al. (2018), suggesting that expectations from modeling studies are presently manifesting in the environment. As was revealed in the modeling analysis of Hauck and Völker (2015), by the end of the 21st century the seasonal cycle of CO_2 uptake over the region south of 30°S (their Figure 1) is anticipated to increase significantly more than the Southern Annular Mode-driven CO_2 flux perturbations described by Lenton and Matear (2007) and Lovenduski et al. (2007). In fact, the changes in seasonality identified by Hauck and Völker (2015) are larger than any known variations in CO_2 fluxes associated with climate variability for the modern era, and may be expected to project onto spatial patterns of surface ocean Revelle factor (RF) perturbations, which are independent of climate mode patterns. If so, future changes in the seasonal cycle of pCO_2 will not be independent of the secular trend in surface ocean anthropogenic carbon content. However, it has not yet been determined whether the sea surface pCO_2 response to anthropogenic carbon accumulation will be a simple amplification of the seasonal cycle in sea-air CO_2 fluxes, with increased summer and winter perturbations largely compensating, or whether one should expect asymmetric responses that could impact the net CO_2 exchange when integrated over the full seasonal cycle. The answer to this question could have important implications for carbon-climate feedbacks, as well as for the evolution of ocean acidification.

In this study, we apply state of the art methods that incorporate both observational and modeling constraints to evaluate how the seasonal cycles of sea surface pCO_2, acidification variables, and the sea-air CO_2 flux respond to the invasion of anthropogenic carbon into the ocean. Motivated by the fact that the Coupled Model Intercomparison Project Phase 5 generation of Earth system models have been shown to exhibit poor fidelity to observed seasonal cycles of surface ocean carbon variables in their phasing and amplitude over many regions (Anav et al., 2013), we choose to begin with observed climatological pCO_2 and acidification variable seasonal cycles inferred from version 4 of the Surface Ocean CO_2 Atlas (Bakker et al., 2016) and centered on the year 2010 (Fassbender, Sabine, & Palevsky, 2017). These climatologies are combined with annual mean secular trends in dissolved inorganic carbon (DIC) from an Earth system model under a

climate change scenario. More specifically, we consider an Earth system model for which the preindustrial radiative balance in the atmosphere is maintained from 1861–2100 (i.e., no anthropogenic warming) while the ocean biogeochemistry module experiences the full evolution of historical/Representative Concentration Pathway 8.5 (RCP8.5) atmospheric CO_2 through its gas exchange boundary condition. This allows us to focus on the thermodynamic ocean carbon cycle perturbations sustained solely by the invasion of CO_2, as a step toward our broader goal of understanding processes modulating the full transient carbon evolution in the ocean.

2. Data

2.1. Observations

Our analysis relies on global monthly climatologies of sea surface: temperature (SST), salinity (SSS), pH, pCO_2, DIC, total alkalinity (TA), and the RF. These climatologies were developed previously by Fassbender, Sabine, and Palevsky (2017) using data from version 4 of the Surface Ocean CO2 Atlas (SOCAT-v4: http://www.socat.info/; Bakker et al., 2016). Briefly, SOCAT-v4 CO_2 data with WOCE quality control flags of 2 (good) and SOCAT metadata flags A through D were downloaded along with the accompanying SSS and SST observations. Applying these quality control flags limits the CO_2 data uncertainty to 5 μatm or less. CO_2 observations were normalized to the year 2010 to remove the anthropogenic trend and data from the equatorial Pacific (between 6°N and 6°S and 130°E and 80°W) were omitted during El Niño years following the approach of Takahashi et al. (2009, 2014). TA was estimated from SOCAT-v4 SST and SSS using equation (8) of the Locally Interpolated Alkalinity Regression (LIAR) suite of algorithms (Carter et al., 2016; TA uncertainty of ~ ±8 μmol/kg) and used with 2010-normalized CO_2 data to calculate additional carbonate system parameters of interest with the MATLAB program CO2SYS version 1.1 (Lewis & Wallace, 1998; van Heuven et al., 2011). The equilibrium constants of Lueker et al. (2000) and Dickson (1990) and the boron-to-chlorinity ratio of Uppström (1974) were used, following the recommendation of Orr et al. (2015), and nutrient concentrations were set to zero for all CO2SYS calculations in this analysis. Data were then gridded to a 3° × 3° scale and averaged by month and then across years to make the 12-month climatologies in each grid cell. Further details about the construction and validation of these climatologies can be found in Fassbender, Sabine, and Palevsky (2017).

This analysis also relies on climatologies developed from long-term observations made at select time series sites, including the Kuroshio Extension Observatory (KEO 32.3°N, 144.5°E; https://www.nodc.noaa.gov/ocads/oceans/Moorings/KEO.html; Fassbender, Sabine, Cronin, & Sutton, 2017), Ocean Station Papa (OSP 50°N, 145°W; https://www.nodc.noaa.gov/ocads/oceans/Moorings/Papa_145W_50N.html; Fassbender et al., 2016), Bermuda Atlantic Time Series Study (BATS 32°N, 64°W; http://bats.bios.edu/), Hawaii Ocean Time Series (HOT 22.75°N, 158°W; http://www.soest.hawaii.edu/HOT_WOCE/index.php), Irminger Sea (64.3°N, 28°W; https://www.nodc.noaa.gov/ocads/oceans/Moorings/Irminger_Sea.html), Iceland Sea (68°N, 12.66°W; http://cdiac.ornl.gov/ftp/oceans/CARINA/IcelandSea//IcelandSea_V2/), and two regions in the Southern Ocean that lie north and south of the Antarctic Polar Front in Drake Passage (DP N 57°S, 64°W; DP S 61.5°S, 62°W; https://www.nodc.noaa.gov/ocads/oceans/VOS_Program/LM_gould.html; Munro et al., 2015). Data from these sites are incorporated due to their high-quality and because some of the associated 3° × 3° SOCAT-v4 grids do not have fully resolved 12-month climatologies due to data scarcity, particularly in the high latitudes (e.g., Irminger and Iceland seas). Further details about the development of these climatologies and how they compare to the SOCAT-v4 climatologies can be found in Fassbender, Sabine, and Palevsky (2017). Finally, 10-m, monthly averaged, global wind speed reanalysis data from the European Centre for Medium-Range Weather Forecasts (ECMWF; Dee et al., 2011; http://www.ecmwf.int/en/research/climate-reanalysis/) are used to calculate sea-air CO_2 fluxes in section 5. ECMWF data were gridded to a 3° × 3° scale and averaged over 1979 to 2015 to create a 12-month wind speed climatology that aligns with the SOCAT-v4 climatology grids. Monthly sea-air CO_2 fluxes (F_{CO2}) were then calculated by applying the parameterization and updated coefficients of Wanninkhof (2014):

$$F_{CO2} = \left[0.251 \times u^2 \times (Sc/660)^{-0.5}\right] \times K_0 \times (pCO_{2\text{ Sea}} - pCO_{2\text{ Air}}) \tag{1}$$

where u is the 10-m wind speed and Sc and K_0 are the CO_2 Schmidt number (Wanninkhof, 1992) and solubility constant (Weiss, 1974), respectively.

2.2. Model Output

The model configuration applied here is the Geophysical Fluid Dynamics Laboratory's (GFDL) Earth system model ESM2M (Dunne et al., 2012, 2013), and the projection considered is derived from a historical and RCP8.5 concentration pathway (Moss et al., 2010; van Vuuren et al., 2011). We use the biogeochemically coupled (BGC; Schwinger et al., 2014) run in which the model follows the full RCP8.5 transient pathway for atmospheric CO_2 mixing ratio over 1861–2100 to drive ocean biogeochemistry via gas exchange. However, with the BGC run, preindustrial atmospheric CO_2 levels are used to drive the radiation component of the model. As such, the BGC run does not include anthropogenically induced warming. The model is monthly resolved and provides output for sea surface variables at a 1° × 1° scale. Data were regridded to the 3° × 3° SOCAT-v4 climatology scale.

BGC model output is used to study long-term changes in ocean carbonate chemistry by applying two different approaches to (A) evaluate the sensitivity of pCO_2 and pH seasonal cycles to anthropogenic carbon accumulation and (B) assess the associated changes in sea-air CO_2 flux. For the former (A), monthly model DIC values from each year were averaged to create an annual time series in each grid, which was smoothed to reduce interannual variability by applying a 4-pass sliding average filter with a 10-year window. The 2010 DIC value was then subtracted from the DIC values for all other years, anchoring the DIC trajectory in each grid to zero at the year 2010. These trajectories were then added to the SOCAT-v4 DIC climatologies such that all projected historical and future DIC changes are relative to the data-based SOCAT-v4 2010 climatology. In this way, the DIC seasonal cycle amplitude (and structure) is maintained, while increases in the annual mean ocean carbon content are incorporated. The 2010-normalized SOCAT-v4 climatologies for TA, SST, and SSS are used with the projected DIC values to calculate pCO_2 and pH seasonal cycles for the years 1861 to 2100 in each grid. This approach isolates the thermodynamic response to anthropogenic carbon invasion under RCP8.5.

A slightly different approach must be used to evaluate changes in the sea-air CO_2 flux (B) since the model displays small transient changes in SSS, SST, and TA (average of 0.02%, −2.7%, and 0.7%, respectively) between 1861 and 2100 as well as small differences in 2010 annual mean DIC values relative to the SOCAT-v4 climatology (average of 1 ± 16 μmol/kg; supporting information Figure S2). These differences must be incorporated into the methodology in order to use the model annual mean air-sea pCO_2 disequilibrium information, which is required to compute sea-air CO_2 fluxes from the calculated monthly sea surface pCO_2 values in section 5. Thus, seasonal anomalies from the annual mean SOCAT-v4 DIC, TA, SSS, and SST climatologies were added to the model trajectories for annual mean DIC, TA, SSS, and SST from the year 1861 to 2100. This approach maintains the seasonal cycle amplitude for DIC, TA, SSS, and SST over time, even as the annual mean values change. Since the transient changes in TA, SSS, and SST are small, this approach primarily captures the thermodynamic carbonate chemistry effect on seasonal pCO_2 variations; however, minor alterations to the physical ocean state also contribute. Use of this modified methodology ensures that the annual mean sea surface pCO_2 matches that of the model, such that the annual mean model disequilibrium between the ocean and atmosphere is accurately reflected in the computed sea-air CO_2 fluxes over the time period 1861 to 2100.

This study is theoretical in nature, so the largest errors come from intentional manipulation of reality by holding the seasonal cycles of specific carbonate system variables constant over time and disallowing anthropogenic warming (Text S1). However, there are also uncertainties associated with the 2010-SOCAT climatologies applied herein. Propagation of these uncertainties through our computations results in a ~30% and ~50% uncertainty in the pCO_2 (and pH) seasonal cycle amplitude in the year 2010 and 2100, respectively (please see Figure S3 and Text S2 for a detailed discussion of methodological uncertainties). Notably, these uncertainties can exceed 100% in regions that presently have low amplitude pCO_2 (and pH) seasonal cycles, such as at the southern Drake Passage site. Setting nutrient values to zero in the CO2SYS calculations contributes an additional uncertainty (≤5%) to the seasonal cycle amplitudes that is negligible in comparison. However, uncertainty in pCO_2 (and pH) values resulting from nutrient omission can be more significant in regions that are naturally nutrient replete (Text S2), such as the Southern Ocean. While these uncertainties may seem large, SOCAT is presently the leading surface ocean CO_2 database in terms of data density (>18 million observations in version 4) and community vetted data quality control (i.e., open, documented protocols). We incorporate the SOCAT-v4 climatology into our analysis to ensure accurate seasonal cycle magnitudes and
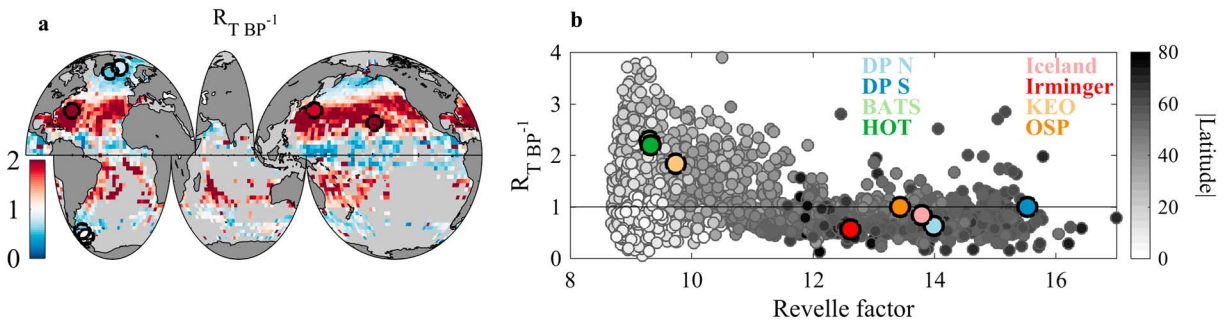
Figure 1. (a) Spatial variability in the dominance of temperature (T) versus biophysical (BP) controls on seasonal pCO_2 variations ($R_{T\ BP^{-1}}$) for SOCAT-v4 grids with at least 4 months of the climatology represented. Values greater than 1 indicate temperature dominance and values less than 1 indicate biophysical dominance. Circles show select time series sites (KEO, OSP, BATS, HOT, Irminger Sea, Iceland Sea, and two regions in Drake Passage located north [DP N] and south [DP S] of the Antarctic Polar Front) and are colored independently of the map. (b) Same as (a) but plotted versus the Revelle factor with latitude (absolute value) shaded in gray. Colored circles and text represent the select time series sites. SOCAT-v4 = Surface Ocean CO_2 Atlas version 4.

phasing, and limit our interpretation of results to ocean regions containing climatology data from at least 4 months of the year. Perhaps more important is that our goal is not to predict future amplification magnitudes but to better understand chemical feedback mechanisms within the carbonate system by gaining insight from large signals over broad ocean regions.

3. Background: Thermodynamic Drivers of Surface Ocean pCO_2 Seasonal Cycles

Seasonal variations in sea surface pCO_2 reflect the competing effects of well-known upper-ocean processes (e.g., Takahashi et al., 1993, 2002). In general, seasonal cooling increases the solubility of CO_2 and reduces sea surface pCO_2 values, which is often counteracted by the input of high DIC (and pCO_2) waters during deep winter mixing. Analogously, seasonal warming decreases the solubility of CO_2 causing pCO_2 values to rise while biological productivity works to reduce pCO_2 as the mixed layer shoals and available nutrients are consumed. These processes are common to nearly all ocean regions, but their magnitudes and timing can vary significantly. To evaluate these seasonally competing controls, the temperature influence can be disentangled from biological and physical (biophysical) processes using the empirical Takahashi et al. (1993, 2002) temperature decomposition:

$$pCO_{2\ T} = pCO_{2\ am} \times \exp[0.0423(T_{mm} - T_{am})] \qquad (2)$$

$$pCO_{2\ BP} = pCO_{2\ mm} \times \exp[0.0423(T_{am} - T_{mm})] \qquad (3)$$

For the purposes of this analysis, the subscripts *T* and *BP* represent temperature and biophysical effects, respectively, while subscripts *am* and *mm* represent annual mean and monthly mean values, respectively. $pCO_{2\ T}$ is derived in equation (2) by imposing the pCO_2 temperature dependency on the annual mean pCO_2 value, while $pCO_{2\ BP}$ is derived in equation (3) by removing the pCO_2 temperature dependency from the observed monthly mean pCO_2 values. Thus, equation (2) provides an estimate of seasonal temperature control over pCO_2 and equation (3) provides an estimate of the residual, biophysical control over pCO_2 (see Text S4; Sarmiento & Gruber, 2006; Takahashi et al., 2002). Biophysical processes include net community production and calcification, sea-air CO_2 exchange, freshwater fluxes, and physical transport and mixing.

The amplitude of $pCO_{2\ T}$ and $pCO_{2\ BP}$ seasonal cycles provides information about the importance of these processes in local pCO_2 variations. Further, the ratio of these amplitudes exposes which processes are most dominant (Takahashi et al., 2002), where

$$R_{T\ BP^{-1}} = \frac{\max(pCO_{2\ T}) - \min(pCO_{2\ T})}{\max(pCO_{2\ BP}) - \min(pCO_{2\ BP})} \qquad (4)$$

$R_{T\ BP^{-1}}$ is displayed in Figure 1a where values greater than 1 indicate that temperature dominates the seasonal pCO_2 cycle, while values less than 1 indicate that biophysical processes dominate. A previously well-described

pattern emerges with temperature controlling seasonal pCO_2 variations in the subtropics and lower temperate latitudes, and biophysical processes driving seasonal pCO_2 variations in the high latitudes and tropics (Takahashi et al., 2002). In the text and analysis that follows, we will show that anthropogenic CO_2 invasion into the ocean also contributes to the seasonal pCO_2 cycle in a way that has thus far received less attention.

The concept of an ocean carbon buffer was first introduced by Revelle and Suess (1957) and has subsequently been expanded upon by numerous investigators (Broecker et al., 1979; Egleston et al., 2010; Frankignoulle, 1994; Sabine et al., 2004; Sundquist et al., 1979; Takahashi et al., 1980) who fittingly ascribed it with the moniker RF. The RF is now commonly used to characterize the buffering capacity of seawater, where RF is defined as the relative change in pCO_2 divided by the relative change in DIC for a given carbonate system perturbation, assuming constant TA:

$$RF = \frac{\partial pCO_2 / pCO_2}{\partial DIC / DIC} \tag{5}$$

In high RF waters only small relative changes in DIC are required to alter the pCO_2 value while large relative changes in pCO_2 are required to alter the DIC concentration. This provides a lever for biophysical processes to be more efficient at modifying pCO_2 in regions with high RF values, since biophysical processes alter the DIC concentration while temperature changes alter pCO_2 but not DIC. For example, consider two hypothetical locations that exhibit the same annual mean pCO_2 and DIC values (e.g., 400 µatm and 2,000 µmol/kg, respectively) but have RF values of 14 and 10. If the spring bloom reduces mixed layer DIC by 20 µmol/kg in both locations, this would cause mixed layer pCO_2 to decline by 52 µatm at the high RF location and by only 38 µatm at the low RF location. This means that spatial variability in RF results in different efficiencies at which biophysical processes influence local pCO_2 dynamics and thus air sea CO_2 exchange. This is shown in Figure 1 b where high-latitude regions with elevated RF values generally exhibit dominance of biophysical processes, while temperature control increases toward the equator (Takahashi et al., 2002). Very close to the equator (lower left quadrant of Figure 1b), biophysical controls dominate over temperature due to the *aqueous CO_2 concentration* effect (Fassbender, Sabine, & Palevsky, 2017), where small changes in DIC cause large changes in pCO_2 due to the naturally elevated pCO_2 DIC^{-1} in this region. Also, the seasonal temperature cycle is quite small near the equator.

An important counterpart to spatial variability in the efficiency at which biophysical processes influence sea surface pCO_2 is variability in how seasonal temperature changes affect seawater pCO_2. The temperature sensitivity of pCO_2 described in equation (2) is dependent on the annual mean pCO_2 value. Therefore, regions with the same magnitude seasonal temperature cycle but differing annual mean pCO_2 values will exhibit different amplitude pCO_2 responses to temperature. For example, consider two regions with seasonal temperature cycles that span 8 to 12 °C, but with annual mean pCO_2 values of 370 and 425 µatm. The associated $pCO_{2\,T}$ amplitudes are ~63 and ~72 µatm, respectively, reflecting a larger temperature response in waters exhibiting higher annual mean pCO_2 values. Thus, similar to how RF is a lever on the efficiency of biophysically driven pCO_2 changes, the annual mean pCO_2 value is a lever for the magnitude of seasonal temperature-driven pCO_2 changes.

To display this concept visually, Figure 2 shows the 2010 annual mean pCO_2, the 2010 seasonal cycle amplitudes (A) of pCO_2, $pCO_{2\,T}$, $pCO_{2\,BP}$, SST, and DIC, and the hypothetical seasonal cycle amplitudes of $pCO_{2\,T}$ and $pCO_{2\,BP}$ that would result if all ocean locations experienced seasonal cycles of ±2.5 °C and ±20 µmol/kg about the annual mean SST and DIC values, respectively (Text S3). While not an accurate representation of seasonal cycle magnitudes, results from the hypothetical simulations clearly exhibit the nonuniform sensitivity of pCO_2 to thermal and biophysical drivers throughout the ocean. A-$pCO_{2\,T}$ (Figure 2c) largely matches A-SST (Figure 2e); however, high annual mean pCO_2 values near the equator (Figure 2a) cause A-$pCO_{2\,T}$ to be slightly elevated in a region of low SST seasonality due to heightened sensitivity (e.g., equation (2) and Figure 2g). Likewise, the pattern of A-$pCO_{2\,BP}$ (Figure 2d) is similar to A-DIC (Figure 2f), but enhanced sensitivity to seasonal DIC changes in regions with elevated RF values (e.g., temperate southern hemisphere; Fassbender, Sabine, & Palevsky, 2017; Sabine et al., 2004) contributes to the modern A-$pCO_{2\,BP}$ (e.g., Figure 2h).

These hypothetical examples indicate that distinct levers dominate seasonal $pCO_{2\,T}$ and $pCO_{2\,BP}$ changes in different ocean regions, and that the modern spatial pattern of A-pCO_2 (Figure 2b) is dependent on multiple

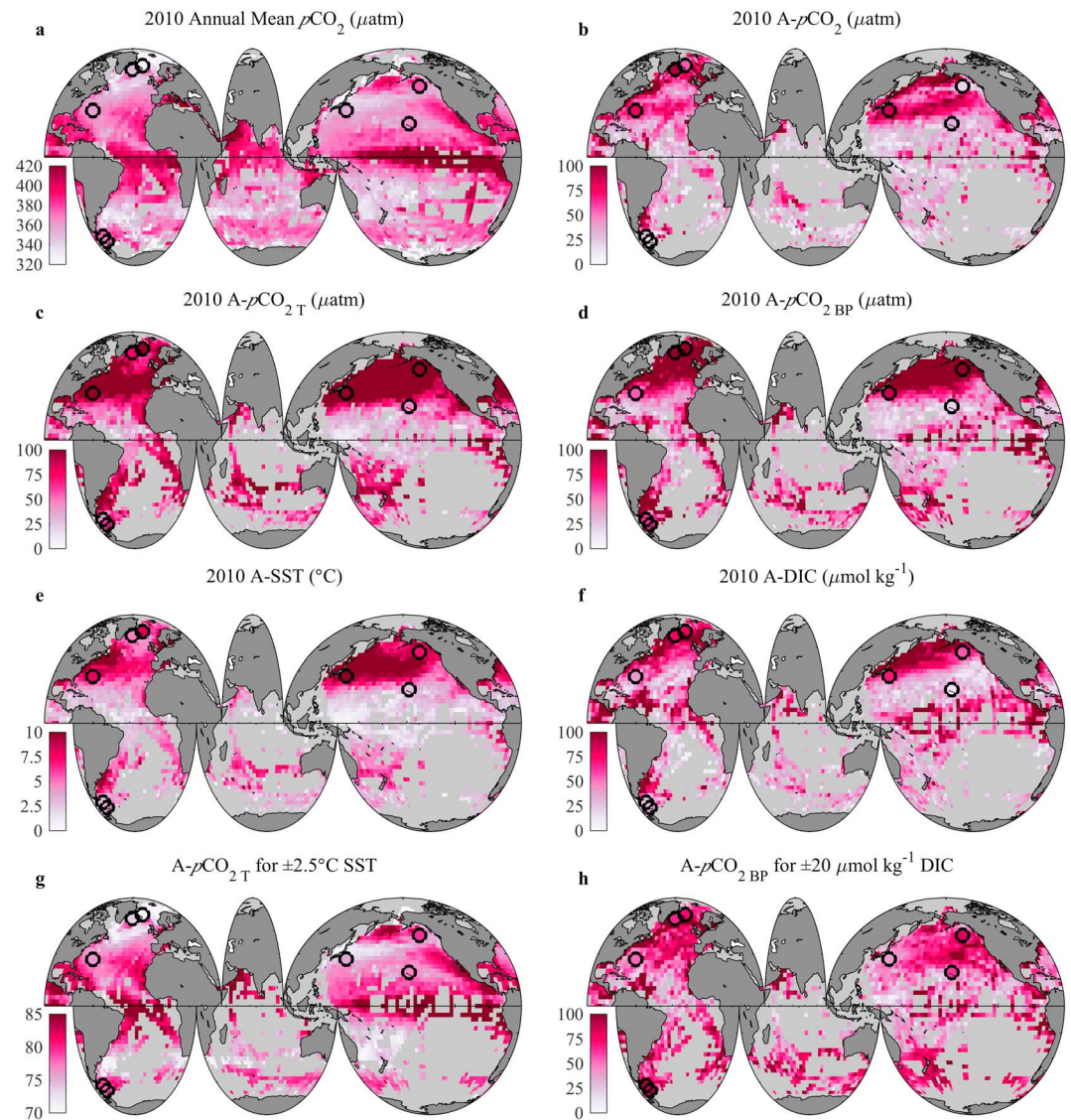**Figure 2.** (a) 2010 annual mean pCO_2 and the seasonal cycle amplitudes (A) of (b) pCO_2, (c) $pCO_{2\,T}$, (d) $pCO_{2\,BP}$, (e) SST, and (f) DIC. Hypothetical seasonal cycle amplitudes of (g) $pCO_{2\,T}$ and (h) $pCO_{2\,BP}$ that would result if all ocean locations experienced seasonal cycles of ±2.5 °C and ±20 μmol/kg about the annual mean SST and DIC values, respectively. SOCAT-v4 grids with at least 4 months of the climatology represented are shown. Circles show select time series sites and are colored independently of the maps. SST = sea surface temperature; DIC = dissolved inorganic carbon; SOCAT-v4 = Surface Ocean CO_2 Atlas version 4.

factors, including ocean chemistry. Notably, the 2010 A-pCO_2 is significantly smaller than the 2010 A-$pCO_{2\,T}$ and A-$pCO_{2\,BP}$, revealing the competing nature of thermal and biophysical processes and indicating that their seasonal timing and magnitude is thus quite important.

4. Thermal and Biophysical Amplification of Surface Ocean pCO_2 and pH Seasonal Cycles

Controls on modern pCO_2 seasonal cycles have been discussed thoroughly in many ocean regions (Körtzinger et al., 2008; McKinley et al., 2006; Takahashi et al., 1993, 2002); however, considerably less emphasis has been given to how the efficiency of these controls will change over time. As a direct consequence of the invasion of anthropogenic CO_2 into the ocean (assuming all else constant, including the SST seasonal cycle amplitude and annual mean value), temperature will begin to exert a larger control on seasonal
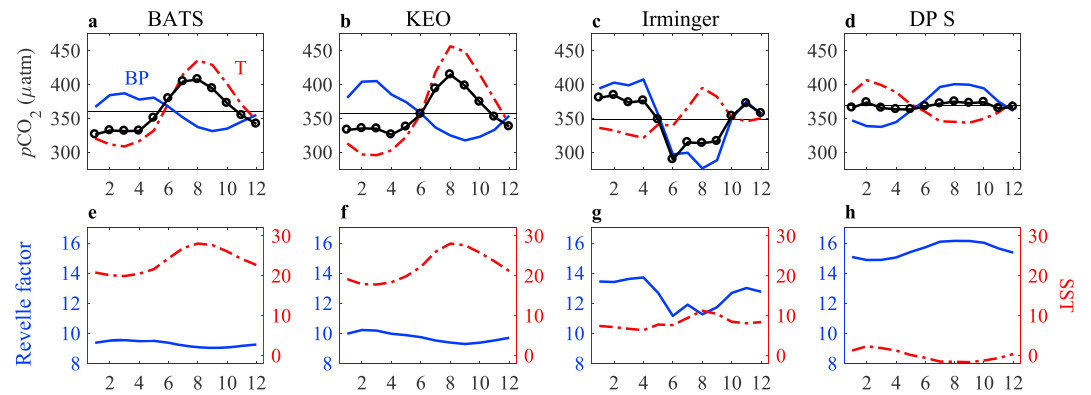
Figure 3. Climatological (a–d) pCO_2 (circles), pCO_2 $_{BP}$, and pCO_2 $_T$ (dashed) seasonal cycles at the BATS, KEO, Irminger Sea, and Southern Drake Passage (DP S) time series sites. Thin horizontal lines show the annual mean pCO_2 value. (e–h) Corresponding Revelle factor and sea surface temperature (dashed) seasonal cycles.

pCO_2 cycles (Gorgues et al., 2010; Nakano et al., 2011; Riebesell et al., 2009; Rodgers et al., 2008). This amplification of the thermal pCO_2 component is dependent on growth in the annual mean pCO_2 (equation (2)), so it will be largest in regions where pCO_2 grows most rapidly. Similarly, as RF values rise, smaller biophysically driven changes in DIC will be required to elicit the same pCO_2 response (Egleston et al., 2010; Hauck & Völker, 2015; Hauck et al., 2015; Riebesell et al., 2009). Therefore, the same magnitude DIC changes resulting from biological productivity and winter mixing will result in amplification of the sea surface pCO_2 cycle, simply due to the accumulation of anthropogenic carbon in the ocean. This concept has also been discussed previously in regard to pH by Riebesell et al. (2009) and Cai et al. (2011).

In a simplistic view where thermal and biophysical processes are perfectly out of phase, an expected result of biophysical component amplification is that seasonal pCO_2 cycles would attenuate in regions presently dominated by temperature (possibly changing the sign of seasonal variations) and would amplify in regions presently dominated by biophysical processes (Egleston et al., 2010; Riebesell et al., 2009). Amplification of the thermal pCO_2 component would be expected to have the opposite effects. Finally, regions presently exhibiting a balance between temperature and biophysical processes would start to express a pCO_2 seasonality that reflects the more dominant amplification process. When evaluating how the modern ocean may respond to these amplification effects there are two important factors to consider. First, pCO_2 $_{BP}$ and pCO_2 $_T$ exhibit different patterns of sensitivity (Figure 2) and amplification will be largest where RF and pCO_2 values rise fastest, respectively (assuming no change in the DIC and SST seasonal cycle amplitudes and annual mean SST). This will result in notable differences in how these competing effects play out over time in various ocean regions. Second, the seasonal timing of thermal and biophysical effects is not always aligned perfectly out of phase, which means that these processes do not seamlessly counteract each other such that amplification of both processes may result in a modified and larger amplitude pCO_2 seasonal cycle.

To evaluate these nonuniform sensitivities, we use observations from well-studied time series sites to illustrate carbonate chemistry responses to rising anthropogenic carbon in the ocean. Figure 3 shows the competing thermal and biophysical effects on seasonal pCO_2 cycles at BATS, KEO, Irminger Sea, and DP S. These sites span much of the global RF domain and exhibit a range of $R_{T\ BP^{-1}}$ values (Figure 1b), providing a cross section of modern ocean conditions. All locations display the opposing effects of temperature and biophysical processes, as well as differences in the dominating process. For example, temperature and biophysical controls are nearly balanced at DP S while temperature dominates at BATS and KEO, and biophysical processes dominate at the Irminger Sea site. These characteristics primarily arise from different annual mean pCO_2 values and seasonal SST ranges, and different annual mean RF values and seasonal DIC ranges associated with winter mixing and spring productivity.

With unique processes dominating across sites, it is reasonable to hypothesize that changes in the seasonal pCO_2 cycle may be regionally distinct under ocean carbon accumulation (assuming all else constant). To theoretically test this idea, pCO_2 and pH were computed from the SOCAT-v4 and time series site SSS, SST, TA, and DIC climatologies while varying the input DIC using the BGC model DIC trajectories from each 3° × 3° grid cell
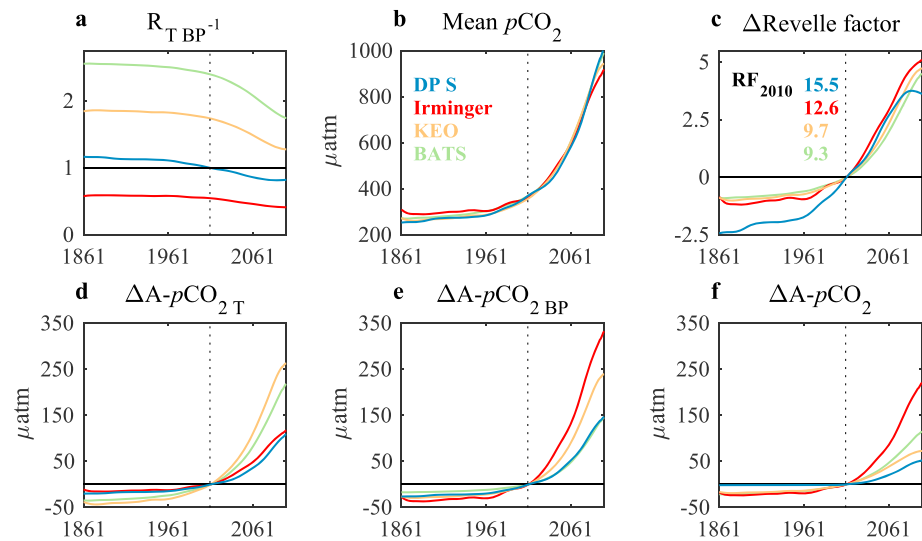
Figure 4. (a) $R_{T\,BP^{-1}}$, annual mean (b) pCO_2 and (c) Revelle factor, and the seasonal cycle amplitudes (A) of (d) $pCO_{2\,T}$, (e) $pCO_{2\,BP}$, and (f) pCO_2 from 1861 to 2100 at the BATS, KEO, Irminger Sea, KEO, and DP S time series sites. Numbers in (c) give the 2010 Revelle factor values at each site. Revelle factor and seasonal cycle amplitudes are plotted relative to (Δ) the 2010 values to more easily compare results across time series sites. Vertical dashed line = 2010.

(approach A in section 2.2; Figure S5b). The resulting pCO_2 values were used with equations (2), (3), and (4) to calculate $pCO_{2\,T}$ and $pCO_{2\,BP}$ and determine $R_{T\,BP^{-1}}$, respectively. Additionally, the resulting pH values were used to determine the slope of the pCO_2-$[H^+]$ relationship (where $[H^+]$ is the hydrogen ion concentration and is equal to 10^{-pH}) so that $pCO_{2\,BP}$ and $pCO_{2\,T}$ could be converted into $[H^+]_{BP}$ and $[H^+]_T$, and subsequently into pH_{BP} and pH_T.

Recall that for this analysis, we choose to vary the annual mean sea surface DIC concentration using BGC model trajectories while maintaining the 2010 SOCAT-v4 climatological DIC seasonal cycle in each grid. This approach is preferred to relying on an atmospheric pCO_2 trajectory and assuming constant sea-air disequilibrium ($pCO_{2\,Sea} - pCO_{2\,Air}$ or $\Delta pCO_{2\,Sea\text{-}Air}$) to invoke sea surface DIC changes, since $\Delta pCO_{2\,Sea\text{-}Air}$ is known to change over time (Hall et al., 2004; Matsumoto & Gruber, 2005; McKinley et al., 2017). A further rationale for using DIC is that increasing the annual mean sea pCO_2 to match atmospheric growth inherently assumes symmetry in the pCO_2 seasonal cycle response to accumulating anthropogenic carbon. This may be why many of the concepts herein have not yet been rigorously evaluated from a data-based approach. Importantly, any model run with monthly resolved sea and air pCO_2 over the time period of interest would have also been appropriate for our analysis; however, the BGC model run is ideal due to the isolation of ocean biogeochemistry changes from the warming and circulation changes caused by radiative effects. Thus, to determine how rising ocean carbon content may magnify seasonal carbon cycle processes, including seaair fluxes, we have elected to modulate the observed annual mean sea surface DIC concentration based on BGC model run results (Figure S2) to study seasonal sensitivities of the carbonate system.

Results from the time series sites are shown in Figure 4 where the year 2010 (vertical dashed line) reflects the observationally based time series site climatology from which perturbations were made. $R_{T\,BP^{-1}}$ declines in all regions (Figure 4a) while the annual mean sea surface pCO_2 rises (Figure 4b), intensifying markedly around 2050 in tandem with atmospheric pCO_2 (Figure S5a) as the ocean works to absorb anthropogenic carbon (Figure S4). This process is accompanied by an associated decline in the ocean buffer capacity that is exhibited by rising RF values (Figure 4c). The intrinsic rate of RF increase with added pCO_2 (i.e., $\partial RF\,\partial pCO_2^{-1}$) is largest for waters that are colder and fresher (Figure 1c of Fassbender, Sabine, & Palevsky, 2017). As a result, RF values in the high latitudes increase most rapidly over time until the rate begins to taper off and change sign, as seen for the DP S site. The peak in RF signifies that the minimum buffer capacity has been reached and that further carbon additions will result in buffer capacity increases (e.g., Egleston et al., 2010). Changes in RF, and the rate at which they occur, will affect how efficiently biophysical processes alter pCO_2 and thus its seasonal cycle amplitude (A). The most rapid growth in A-$pCO_{2\,BP}$ occurs at the Irminger Sea site (Figure 4e), which

exhibits the largest seasonal biological DIC drawdown in addition to an elevated annual mean RF value (Figure 3). The most rapid growth in A-pCO$_{2\ T}$ occurs at the KEO site, which exhibits the largest seasonal SST cycle (Figure 3). At DP S, the rates of amplification in thermal and biophysical components of pCO$_2$ seasonality are effectively balanced until ~2020 (Figure 4f), leading to no change in A-pCO$_2$ until amplification of the biophysical component outpaces that of the thermal component. The A-pCO$_2$ increases are not necessarily equal to the difference between A-pCO$_{2\ T}$ and A-pCO$_{2\ BP}$ since the seasonal timing of pCO$_2$ drivers is not always perfectly aligned.

While A-pCO$_2$ growth may be anticipated in locations moving away from R$_{T\ BP^{-1}}$ = 1, it is not intuitive in regions moving toward R$_{T\ BP^{-1}}$ = 1 where we might anticipate attenuation in A-pCO$_2$ as competing thermal and biophysical processes get closer to having the same amplitudes. DP S exhibits the expected behavior, where A-pCO$_2$ is relatively stagnant until after R$_{T\ BP^{-1}}$ crosses the equivalence threshold (R$_{T\ BP^{-1}}$ = 1). This is not the case at BATS and KEO, where A-pCO$_2$ continues to grow as R$_{T\ BP^{-1}}$ approaches 1. There are two possible reasons for sustained A-pCO$_2$ growth as R$_{T\ BP^{-1}}$ approaches 1. First, as mentioned previously, thermal and biophysical processes will not perfectly counteract each other if their seasonal cycle timing is offset, which can allow growth in one amplification process to cause growth in the total A-pCO$_2$. Second, amplification of the thermal and biophysical components does not always occur at the same rate. Unlike the DP S and Irminger sites, BATS and KEO display larger amplification of the thermal pCO$_2$ seasonal cycle component (Figures 4d and 4e) and the R$_{T\ BP^{-1}}$ values only decline at BATS and KEO due to simultaneous increases in A-pCO$_{2\ T}$ and A-pCO$_{2\ BP}$. Consider a location that has a starting A-pCO$_{2\ T}$ of ~100 and A-pCO$_{2\ BP}$ of ~50, yielding an initial R$_{T\ BP^{-1}}$ of 2. If the thermal amplitude grows by 50 μatm and the biophysical amplitude grows by 40 μatm, R$_{T\ BP^{-1}}$ becomes 1.7. This is a decrease in R$_{T\ BP^{-1}}$, even though the increase in A-pCO$_{2\ T}$ is greater than that of A-pCO$_{2\ BP}$, highlighting that R$_{T\ BP^{-1}}$ simply reflects the process of dominance at a given time and trends in R$_{T\ BP^{-1}}$ provide information about which process is experiencing larger relative growth.

Results for pH are shown in Figures 5a–5d where annual mean pH values decline in all regions, with the largest change at DP S where pCO$_2$ and RF grow fastest. Much like for pCO$_2$, temperature fluctuations dominate the 2010 pH seasonal cycles at BATS and KEO while biophysical processes dominate at the Irminger Sea site, and dynamics are in balance at DP S leading to a muted pH seasonal cycle (Figure S6). Interestingly, A-pH$_{BP}$ increases over time at each site while A-pH$_T$ increases at Irminger and DP S but declines at BATS and KEO (Figures 5 and S7). This counterintuitive result can be understood by considering how the results for pCO$_2$ translate to [H$^+$]. Since the seasonal temperature range at each site is fixed to the SST climatology, A-pCO$_{2\ T}$ increases in constant proportion with pCO$_{2\ am}$, following equation (2). On the other hand, A-pCO$_{2\ BP}$ is primarily governed by the seasonal DIC cycle and rising RF values, becoming a larger fraction of pCO$_{2\ am}$ over time (Table S1). Due to the strong linear relationship between pCO$_2$ and [H$^+$], we can use pCO$_2$ to see how these effects translate to [H$^+$], where

$$[H^+] = m \times p\text{CO}_2 + b \tag{6}$$

Here, m is the slope and b is the intercept of the linear relationship between pCO$_2$ and [H$^+$] at each site and model time step. Using equation (6) we can evaluate how A-[H$^+$]$_T$ varies with [H$^+$]$_{am}$:

$$\frac{A\text{-}[H^+]_T}{[H^+]_{am}} = \frac{(m \times \max(p\text{CO}_{2\ T}) + b) - (m \times \min(p\text{CO}_{2\ T}) + b)}{(m \times p\text{CO}_{2\ am} + b)} \tag{7}$$

$$\frac{A\text{-}[H^+]_T}{[H^+]_{am}} = \frac{m \times (\max(p\text{CO}_{2\ T}) - \min(p\text{CO}_{2\ T}))}{(m \times p\text{CO}_{2\ am} + b)} \tag{8}$$

$$\frac{A\text{-}[H^+]_T}{[H^+]_{am}} = \frac{m \times A - p\text{CO}_{2\ T}}{(m \times p\text{CO}_{2\ am} + b)} \tag{9}$$

$$\frac{A\text{-}[H^+]_T}{[H^+]_{am}} = \frac{A - p\text{CO}_{2\ T}}{(p\text{CO}_{2\ am} + b/m)} \tag{10}$$

Unlike for pCO$_{2\ T}$, A-[H$^+$]$_T$ does not grow in constant proportion to the annual mean value ([H$^+$]$_{am}$), which would result in a constant A-pH$_T$ value over time. Instead, the proportion is variable through the b/m term
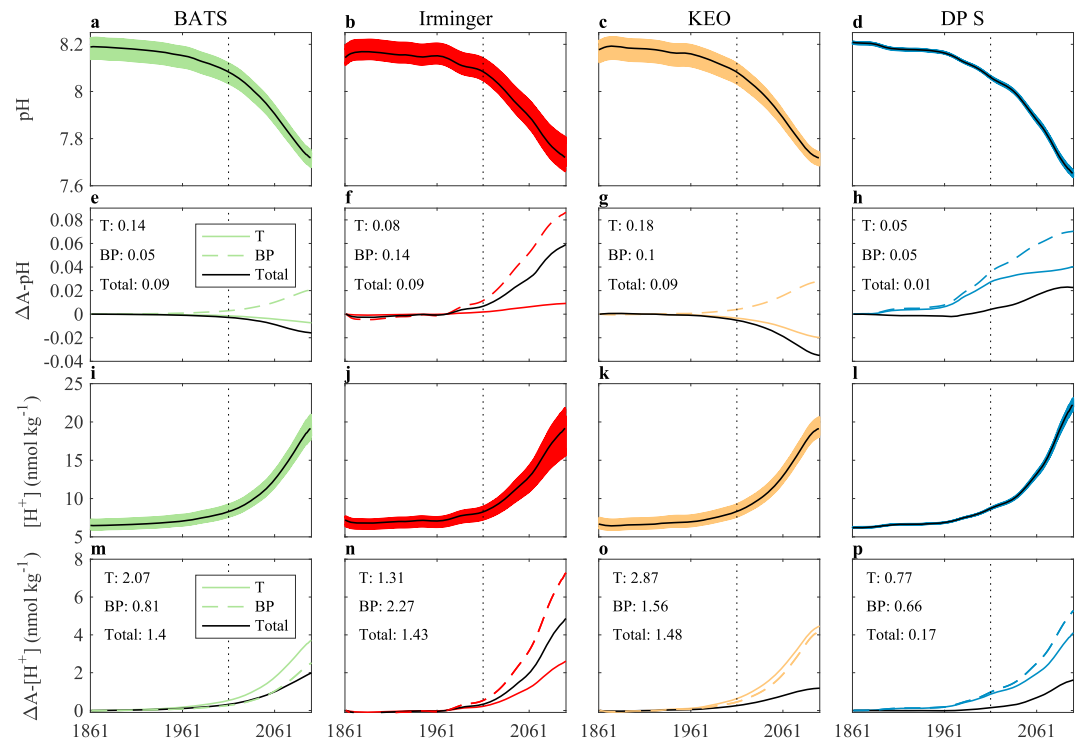
Figure 5. Evolution of (a–d) pH and (i–l) [H$^+$] (with monthly values shown in color) and the seasonal cycle amplitudes (A) of (e–h) pH, pH$_T$, and pH$_{BP}$ and (m–p) [H$^+$], [H$^+$]$_T$, and [H$^+$]$_{BP}$ from 1861 to 2100 at the BATS, KEO, Irminger Sea, KEO, and DP S time series sites. Black lines in (a)–(d) and (i)–(l) represent annual mean values. Seasonal cycle amplitudes are plotted as changes (Δ) relative to 1861 to more easily compare results across time series sites. Amplitudes for the year 1861 are listed in subplots (e)–(h) and (m)–(p). Vertical dashed line = 2010.

in equation (10), indicating that the sensitivity of [H$^+$] to pCO$_2$ is not constant (equation (6); Table S1). We find that A-[H$^+$]$_T$ [H$^+$]$_{am}$$^{-1}$ decreases in regions presently dominated by temperature (e.g., BATS and KEO) resulting in corresponding declines in A-pH$_T$ (Table S1). Meanwhile, A-[H$^+$]$_{BP}$ [H$^+$]$_{am}$$^{-1}$ increases over time at all four time series sites causing A-pH$_{BP}$ to increase. The result of decreasing A-pH$_T$ and increasing A-pH$_{BP}$ in regions presently dominated by temperature is a decline in the total A-pH (Figures 5 and S7 and Table S1). At locations where biophysical processes presently dominate (e.g., Irminger), A-pH$_{BP}$ also outpaces A-pH$_T$ (though both are increasing in this case) causing A-pH to increase. At DP S, there is initially a small decline in A-pH as biophysical processes erode the temperature driven seasonality until the region transitions from weak thermal dominance to biophysical dominance (Figures 4a and 5), at which point A-pH grows by taking on the opposite seasonality.

Temporal changes in ocean acidity are significantly more intuitive when viewed in [H$^+$] space (Figures 5i–5p) where it is easier to identify the dominating amplification process. Additionally, it becomes clear that the overall amplification (A-[H$^+$]) is largest at locations with more significant differences between thermal and biophysical amplification (e.g., Irminger), which work to counteract each other. Much like A-pCO$_2$, A-[H$^+$] is not equal to the difference between A-[H$^+$]$_T$ and A-[H$^+$]$_{BP}$ since the seasonal timing is not always perfectly aligned. For BATS and KEO, the larger magnitude amplification of A-[H$^+$]$_T$ versus A-[H$^+$]$_{BP}$ is now apparent (Figure 5) and there is a clear increase in the total A-[H$^+$] with time. However, when translated to the pH scale, the slower rate of growth in A-[H$^+$] relative [H$^+$]$_{am}$ yields a decline in A-pH, which could be misinterpreted as a reduction in the seasonal range of ocean acidity if one is not careful to consider the contemporaneous decrease in pH$_{am}$. This highlights a potential deficiency in using pH to describe changes in acidity over time.

To evaluate these amplification processes on a global scale, Figure 6 shows the change (Δ) in A-pCO$_2$ $_T$ divided by the change in A-pCO$_2$ $_{BP}$ (ΔA-pCO$_2$ $_T$ ΔA-pCO$_2$ $_{BP}$$^{-1}$), as well as the changes in A-pCO$_2$, A-pH, and A-[H$^+$] from 1861 to 2010 and from 2010 to 2100. The large-scale patterns of ΔA-pCO$_2$ $_T$ ΔA-pCO$_2$ $_{BP}$$^{-1}$
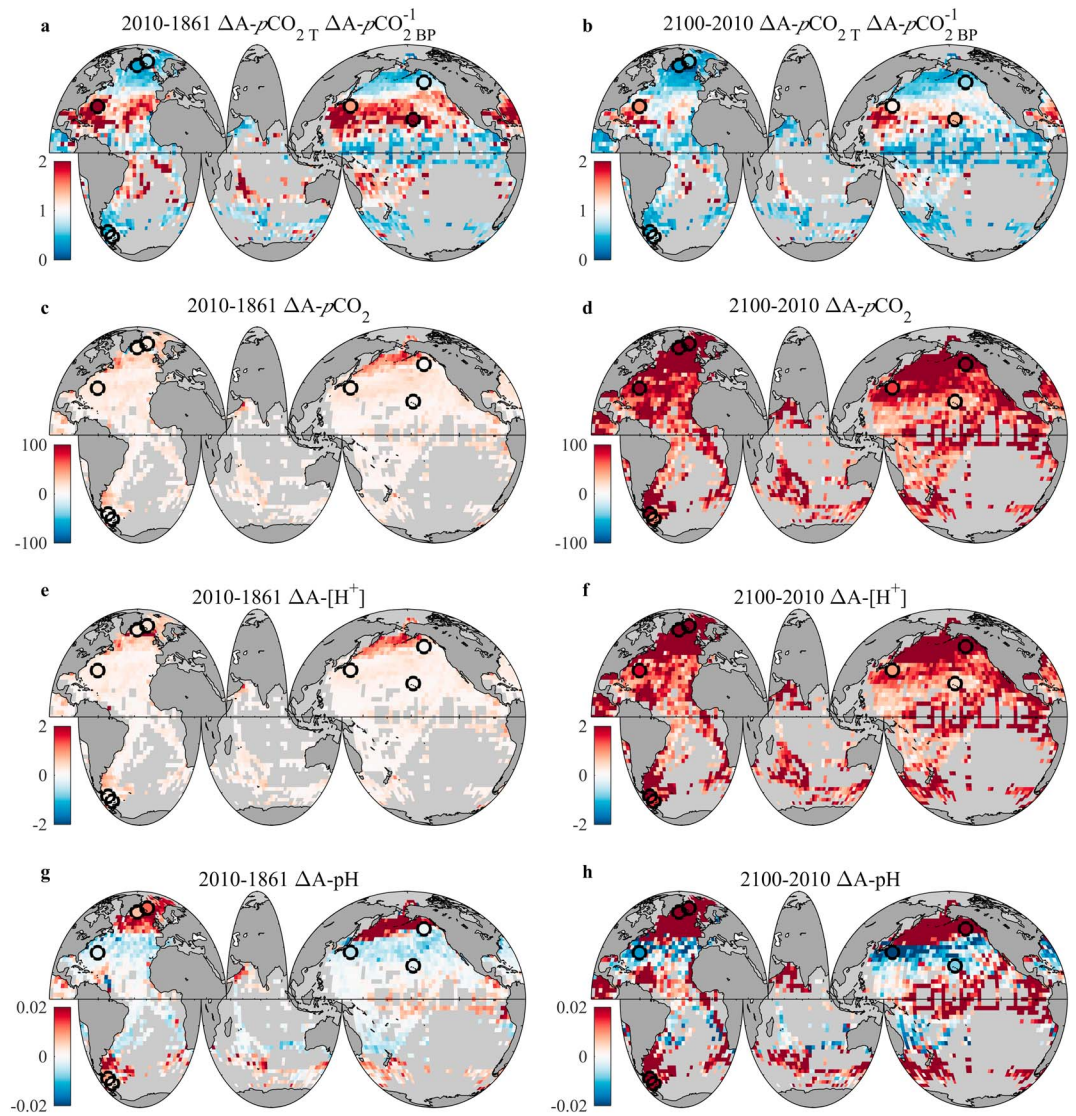
Figure 6. 1861 to 2010 (left panels) and 2010 to 2100 (right panels) changes in the seasonal cycle amplitudes (ΔA) of (a–b) pCO$_{2\,T}$ pCO$_{2\,BP}^{-1}$, (c–d) pCO$_2$ (μatm), (e–f) [H$^+$] (nmol/kg), and (g–h) pH in SOCAT-v4 grids with at least 4 months of the climatology represented. Circles show select time series sites and are colored independently of the maps. SOCAT-v4 = Surface Ocean CO$_2$ Atlas version 4.

in Figures 6a and 6b are similar to the 2010 R$_{T\,BP^{-1}}$ (Figure 1a) indicating that amplification of the thermal component is generally larger than amplification of the biophysical component in ocean regions where pCO$_2$ variations are presently dominated by seasonal temperature changes (also see Figure S8). Similarly, amplification of the biophysical component is generally larger in areas presently dominated by biophysical processes. Interestingly, the magnitude of ΔA-pCO$_{2\,T}$ ΔA-pCO$_{2\,BP}^{-1}$ is larger from 1861 to 2010 than from 2010 to 2100 in the subtropics, which suggests more rapid amplification of the biophysical component than the thermal component from 2010 to 2100 in these regions (under the assumption of no change to the 2010 annual mean SST value and seasonal cycle amplitudes of SST and DIC).

As a result of this global amplification pattern, ΔA-pCO$_2$ (Figures 6c and 6d) and ΔA-[H$^+$] (Figures 6e and 6f) are greater than zero in nearly all regions (where data are available) since the presently dominating control is maintained or amplified through 2100. Over shorter time scales it is likely that seasonal cycle amplitudes would decline in regions transitioning from thermal to biophysical dominance, or vice versa, such as near the equatorward and poleward boundaries of the subtropical gyres. As expected, the patterns of ΔA-pCO$_2$

(Figures 6c and 6d) and ΔA-[H$^+$] (Figures 6e and 6f) are nearly identical and show the largest changes in the high latitudes due to elevated RF values and in the equatorial Pacific due to the *aqueous CO$_2$ concentration* effect (naturally high pCO$_2$ DIC^{-1}; Fassbender, Sabine, & Palevsky, 2017). Finally, ΔA-pH (Figures 6g and 6h) increases in the high latitudes and equatorial Pacific and displays a coherent pattern of decline in the temperate latitudes of both hemispheres. Similar to the findings at KEO and BATS, attenuation of A-pH results from growth in A-pH$_{BP}$ and a decline in A-pH$_T$ (Figures 5 and S6). Thus, ocean regions in which the pCO$_2$ seasonal cycle is driven by temperature will exhibit attenuation in the seasonal pH range as carbon accumulates, in the absence of changes to all other processes. Importantly, even though A-pH will decline, the seasonal acidity range will increase (Figures 5 and 6). Prior investigators have acknowledged the potential for A-pH amplification (Egleston et al., 2010; Frankignoulle et al., 1994; Hagens et al., 2015; Riebesell et al., 2009); however, we find that A-pH attenuation may also be a possibility in the subtropical gyres.

In summary, the ocean's accumulation of anthropogenic carbon causes nonlinear changes in the seasonal cycle amplitudes of pCO$_2$, pH, and [H$^+$] (Figures 5 and 6). Biophysical and thermal pCO$_2$ component amplification is largest in regions where the associated process already dominates seasonal pCO$_2$ variations. As a result, A-pCO$_2$ and A-[H$^+$] are maintained or grow in nearly all ocean regions with increasing DIC. Locations where the thermal and biophysical pCO$_2$ components amplify at the same rate (e.g., DP S), or there is a transition in the dominant control, can lead to negligible changes or declines in A-pCO$_2$ and A-[H$^+$], indicating that the time horizon of the analysis is an important consideration.

5. Seasonal Asymmetry in the Evolution of Sea-Air CO$_2$ Fluxes

Given our interest in addressing the implications for climate (sea-air exchange of CO$_2$), we consider next the degree to which there are asymmetries in the amplification of pCO$_2$ and CO$_2$ fluxes under the invasion of anthropogenic CO$_2$. Amplification of the thermal pCO$_2$ component depends on the annual mean sea surface pCO$_2$ value and the magnitude of seasonal SST variations (equation (2)), which is held constant in this analysis. Amplification of the biophysical pCO$_2$ component depends on seawater RF characteristics and the magnitude of seasonal DIC variations, where the DIC seasonal cycle is held constant in this analysis even as increases in the annual mean DIC are imposed. How the amplification processes evolve under anthropogenic carbon accumulation thus depends on the rates at which sea surface pCO$_2$ and RF increase. Importantly, the RF varies seasonally and is highest during winter and lowest during summer (Figures S6 and S9), which means that DIC changes of the same magnitude will have a larger influence on pCO$_2$ during winter than summer, resulting in seasonal asymmetry to the amplification of the biophysical component.

The amplitude of the RF seasonal cycle (A-RF) depends primarily on seasonal DIC and TA concentration changes. In many ocean areas, the seasonal cycle of DIC is large relative to TA; therefore, regions with large (small) A-DIC generally experience large (small) A-RF. Further, A-RF is nonstationary under increasing anthropogenic carbon accumulation (Figure S10a; Hauck & Völker, 2015), which could play an important role in the way that amplification processes and sea-air CO$_2$ fluxes evolve over time. Growth in A-RF may cause large discrepancies in the influence of winter mixing versus summer biological productivity on pCO$_2$, even if the mixed layer DIC change during each season is identical in magnitude (Figure S10b). Since winter mixing counteracts the effects of cooling on pCO$_2$, A-RF growth would work to erode (enhance) the sea-air CO$_2$ sink (source) strength in locations where temperature (mixing) dominates during winter. Rising RF values will also increase the efficiency of biology at reducing pCO$_2$ during spring and summer; however, at a slower rate than would occur if A-RF did not increase over time.

To evaluate how these amplification processes influence sea-air CO$_2$ fluxes (F$_{CO2}$) we use the modified BGC model approach described in section 2.2 (approach B), which incorporates the small transient changes in model annual mean SSS, SST, and TA in order to accurately apply the model annual mean disequilibrium term. The computed sea surface pCO$_2$ values are used with the ECMWF wind speed climatology (described in section 2.2) to solve equation (1) over the study period. By using a wind speed climatology and fixed amplitude SSS, SST, TA, and DIC seasonal cycles, any temporal changes in the sea-air CO$_2$ flux result from the annual mean offset between air and sea pCO$_2$ (ΔpCO$_2$ $_{Sea-Air}$; as determined from the model annual mean disequilibrium, with negative values indicating fluxes into the ocean), as well as any asymmetric changes in the seawater pCO$_2$ seasonal cycle that are primarily caused by anthropogenic carbon accumulation. The results were
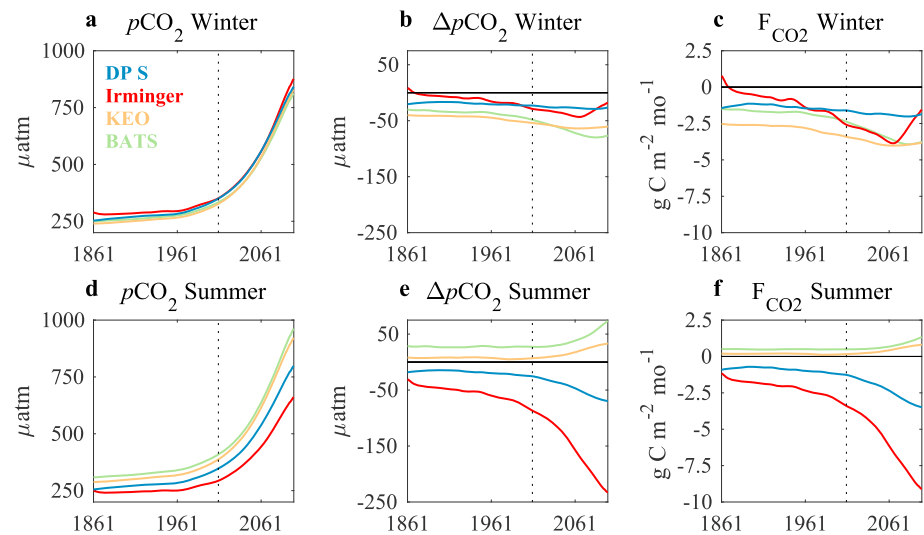
Figure 7. (a–c) Winter and (d–f) summer pCO_2, ΔpCO_2 $_{Sea-Air}$ (where Δ here represents the sea-air disequilibrium), and sea-air CO_2 flux (F_{CO2}) from 1861 to 2100 at the BATS, KEO, Irminger Sea, KEO, and DP S time series sites. Vertical dashed line = 2010. Winter (summer) is defined as January through March in the northern (southern) hemisphere and July through September in the southern (northern) hemisphere.

averaged from January through March and from July through September of each year to evaluate seasonal changes in F_{CO2} over time and are shown in Figure 7. Seasonal differences in sea surface pCO_2 growth (Figures 7a and 7d) lead to seasonal differences in ΔpCO_2 $_{Sea-Air}$ (Figures 7b and 7e). At the Irminger and DP S sites, ΔpCO_2 $_{Sea-Air}$ displays larger changes during summer than winter through 2100, while the seasonal changes in ΔpCO_2 $_{Sea-Air}$ are of comparable magnitude at BATS and KEO. Faster wind speeds at the high latitudes and during winter (Figure S11) result in more efficient gas transfer (e.g., Wanninkhof, 2014), causing notable differences in how ΔpCO_2 $_{Sea-Air}$ translates to F_{CO2} across sites (Figures 7c and 7f). This is particularly apparent for the winter season where the smaller ΔpCO_2 $_{Sea-Air}$ at the Irminger site yields fluxes equivalent to those at BATS in the early 21st century.

Next, we consider the degree of asymmetry in winter and summer perturbations to pCO_2 and sea-air CO_2 fluxes. The results for pCO_2 are shown in Figure 8, where asymmetries in the thermal and biophysical components are evaluated at the four time series sites. There is clear seasonal asymmetry in how pCO_2 $_T$ and pCO_2 $_{BP}$ change with time, with larger growth in the pCO_2 $_T$ summer maximum than winter minimum (black lines in Figures 8a–8d) and larger growth in the pCO_2 $_{BP}$ winter maximum than summer minimum (black lines in Figures 8e–8h). This can be seen more clearly in Figures 8i–8l as the difference between the seasonal maximum and minimum values for pCO_2 $_T$ and pCO_2 $_{BP}$. If there were no change in amplitude of the pCO_2 $_T$ and pCO_2 $_{BP}$ seasonal cycles over time, the lines would be flat.

To better characterize the unique evolutions of pCO_2 $_T$ and pCO_2 $_{BP}$ seasonal extrema, we identified the month during which SST deviates least from the annual mean SST value using the time series site 2010 climatologies. This month serves as a guide for when changes to pCO_2 $_T$ are smallest (Figure S6). We then subtracted the pCO_2 $_T$ value during this neutral month (white line Figures 8a–8d) from the seasonal extrema (black lines in Figures 8a–8d) and determined the percentage growth in the seasonal maximum and minimum values from 1861 to 2100, relative to the neutral month. The finding of equal percentage growth (Figures 8a–8d ΔMax and ΔMin values) in pCO_2 $_T$ maximum and minimum values suggests that amplification of the thermal pCO_2 component is linear in nature, as expected from equation (2), where the annual mean pCO_2 is simply a multiplier. However, the absolute magnitude of seasonal extrema amplification depends on asymmetry in the SST seasonal cycle (Figure S6a), which results in larger magnitude excursions during the summer season at all of the time series sites considered.

To evaluate amplification of the biophysical pCO_2 component, which is expected to exhibit nonlinear behavior as a result of seasonality and growth in RF (Figure S10), we identified the month during which salinity normalized DIC (nDIC) deviates least from the annual mean nDIC value using the time series site 2010
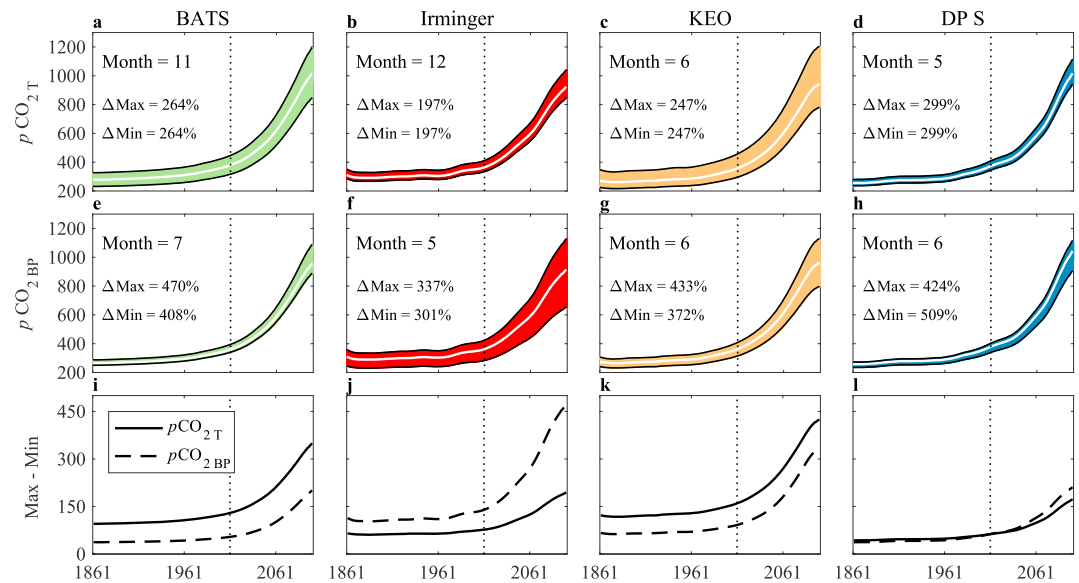
AGU
100
ADVANCING EARTH
AND SPACE SCIENCE

Global Biogeochemical Cycles

10.1029/2017GB005855

Figure 8. Evolution of (a–d) $pCO_{2\ T}$ and (e–h) $pCO_{2\ BP}$ (with monthly values shown in color) and the associated (i–l) differences between seasonal maximum and minimum $pCO_{2\ T}$ and $pCO_{2\ BP}$ values from 1861 to 2100 at the BATS, KEO, Irminger Sea, KEO, and DP S time series sites. White lines in subplots (a)–(d) represent the $pCO_{2\ T}$ values during the month (noted in the subplot) in which the smallest deviation from the annual mean sea surface temperature occurs. White lines in subplots (e)–(h) represent the $pCO_{2\ BP}$ values during the month (noted in the subplot) in which the smallest deviation from the annual mean nDIC occurs. ΔMax and ΔMin refer to the percentage change in the seasonal maxima and minima, relative to the neutral month, from 1861 to 2100.

climatologies. This month serves as a guide for when changes to $pCO_{2\ BP}$ are smallest (Figure S6f). We then subtracted the $pCO_{2\ BP}$ value during this neutral month (white line Figures 8e–8h) from the seasonal extrema (black lines in Figures 8e–8h) and determined the percentage growth in the seasonal maximum and minimum values from 1861 to 2100, relative to the neutral month. The resulting percentage growth in seasonal extrema is not symmetrically distributed around the neutral $pCO_{2\ BP}$ month. The percent change in the seasonal maximum is larger than that of the seasonal minimum at BATS, Irminger, and KEO, while the percent change in the seasonal minimum is larger than that of the seasonal maximum at DP S. This confirms that growth in RF and amplification of the RF seasonal cycle over time results in an enhanced sensitivity of pCO_2 to changes in DIC that is seasonally asymmetric and region specific, causing nonlinear amplification of $pCO_{2\ BP}$ seasonal cycles. Notably, the absolute magnitude of $pCO_{2\ BP}$ seasonal extrema growth depends on asymmetries in, and complex interactions between, the DIC and RF seasonal cycles, which can cause larger magnitude excursions during either summer or winter, depending on location.

In summary, the results indicate that $pCO_{2\ T}$ and $pCO_{2\ BP}$ values are highest and grow fastest during the season in which the associated process (e.g., warming, biology, and mixing) facilitates a reduced (enhanced) ocean CO_2 sink (source) strength. However, because thermal and biophysical processes are antagonistic, the seasonal effects are muted in terms of pCO_2 and $\Delta pCO_{2\ Sea-Air}$ (Figure 7). Dominance of $pCO_{2\ T}$ amplification at BATS and KEO (Figures 8i and 8k) results in enhancement of the winter sink strength and summer source strength over time until nonlinear $pCO_{2\ BP}$ amplification begins to counteract the effect, particularly during winter (Figure 7b). The role of $pCO_{2\ T}$ seasonal cycle amplification in enhancing wintertime subtropical sink strengths has been discussed previously by Rodgers et al. (2008), Gorgues et al. (2010), and Nakano et al. (2011). Over longer timescales, however, it appears that this sink enhancement may not persist under the RCP8.5 concentration pathway (and no anthropogenic warming) due to the ability of nonlinear $pCO_{2\ BP}$ seasonal cycle amplification to effectively "catch up" to the linear $pCO_{2\ T}$ seasonal cycle amplification (e.g., Figures 8k and 8l). Dominance of $pCO_{2\ BP}$ seasonal cycle amplification at Irminger causes this location to be a strong summertime sink for CO_2 that grows over time (Figure 7e). The winter sink strength also grows with time until $pCO_{2\ BP}$ amplification overtakes $pCO_{2\ T}$ amplification (e.g., Figures 8b and 8f) and the winter sink begins to erode (Figure 7c). The results from Irminger highlight the importance of timing and asymmetry
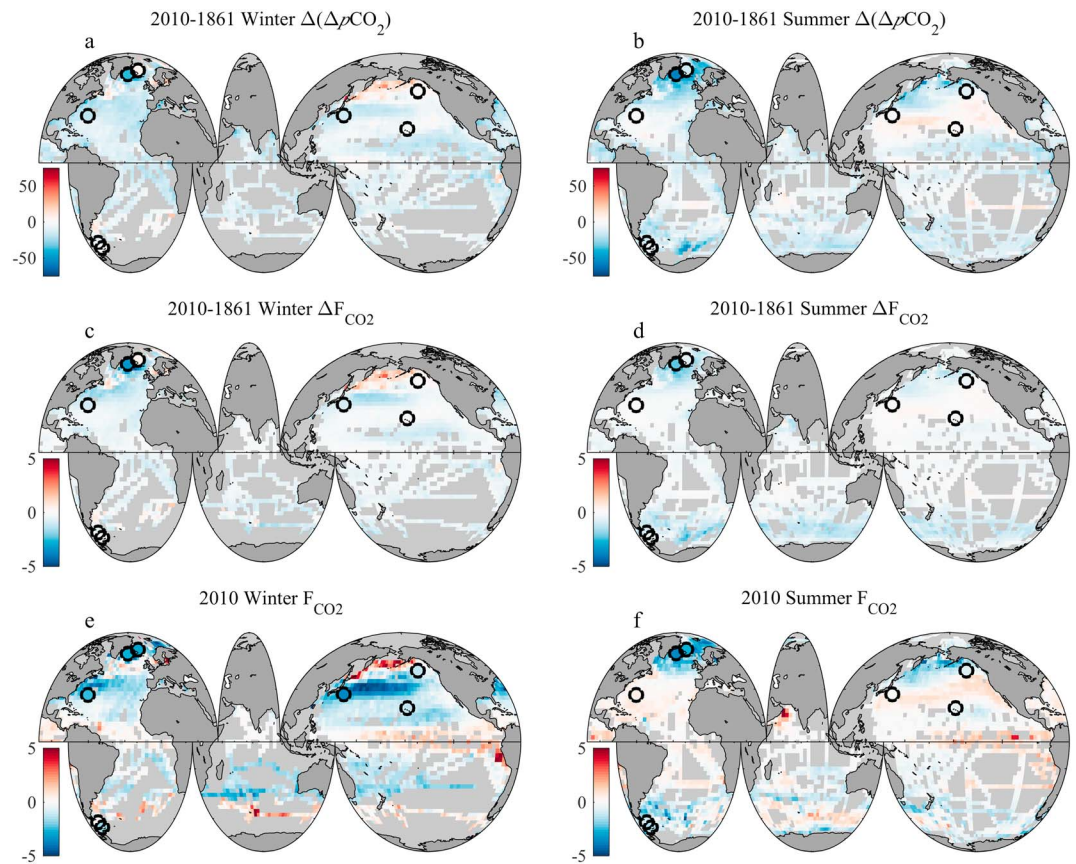
Figure 9. Changes in winter and summer (a–b) ΔpCO_2 $_{\text{Sea-Air}}$ (µatm) and (c–d) sea-air CO_2 flux (F_{CO2}; g C m^{-2} mo^{-1}) from 1861 to 2010. Winter (summer) is defined as January through March in the northern (southern) hemisphere and July through September in the southern (northern) hemisphere. (e) 2010 winter and (f) summer sea-air CO_2 flux (F_{CO2}; g C m^{-2} mo^{-1}). Data are plotted for SOCAT-v4 grids with at least 4 months of the climatology represented. Circles show select time series and are colored independently of the maps. In panels (a)–(d), red indicates a reduced sink or enhanced source and blue indicates an enhanced sink or reduced source. SOCAT-v4 = Surface Ocean CO_2 Atlas version 4.

in the seasonal processes that influence pCO_2. Irminger exhibits a strong biophysical dominance (Figures 1a $R_{T\ BP^{-1}} < 1$ and S8) but it is largely expressed during summer, while cooling outcompetes biophysical processes during winter. This allows the Irminger site to be a CO_2 sink year-round. Similarly, balance between thermal and biophysical control over pCO_2 at DP S causes this site to remain a relatively steady winter and summer CO_2 sink (Figures 7c and 7f) until biophysical processes take on a more dominant role and lead to enhanced sink during summer as biological DIC drawdown is amplified. The site is able to maintain its winter sink strength due to the larger influence of seasonal cooling than mixing on pCO_2, even as biophysical processes start to dominate (Figure 4a). The findings at Irminger and DP S reveal that a larger amplitude seasonal cycle in pCO_2 $_{BP}$ versus pCO_2 $_T$ (or vice versa) does not necessarily equate to biophysical (thermal) dominance during both summer and winter, and thus, $R_{T\ BP^{-1}}$ does not provide information about the time of year that biophysical or thermal processes dominate pCO_2 variations. Importantly, although our focus is on pCO_2, the linear relationship between pCO_2 and [H$^+$] indicates that these asymmetries also hold true for ocean acidification, as recently discussed for estuarine habitats by Pacella et al. (2018). Further investigation of seasonally asymmetric [H$^+$] (and pH) changes in fully coupled model runs and observations is needed to assess the implications for ocean ecosystems, building on prior work by Kwiatkowski & Orr, 2018; McNeil & Sasse, 2016; Sasse et al., 2015; Shaw et al., 2013, and others.

To assess whether the time series site results are representative of broader regional responses, we now look at the global pattern of changes in pCO_2, ΔpCO_2 $_{\text{Sea-Air}}$, and F_{CO2}. Global changes in seasonal ΔpCO_2 $_{\text{Sea-Air}}$ and sea-air fluxes from 1861 to 2010 are shown in Figures 9a–9d. The winter and summer ΔpCO_2 $_{\text{Sea-Air}}$ changes are similar in magnitude but have unique spatial patterns that generally match expectations from
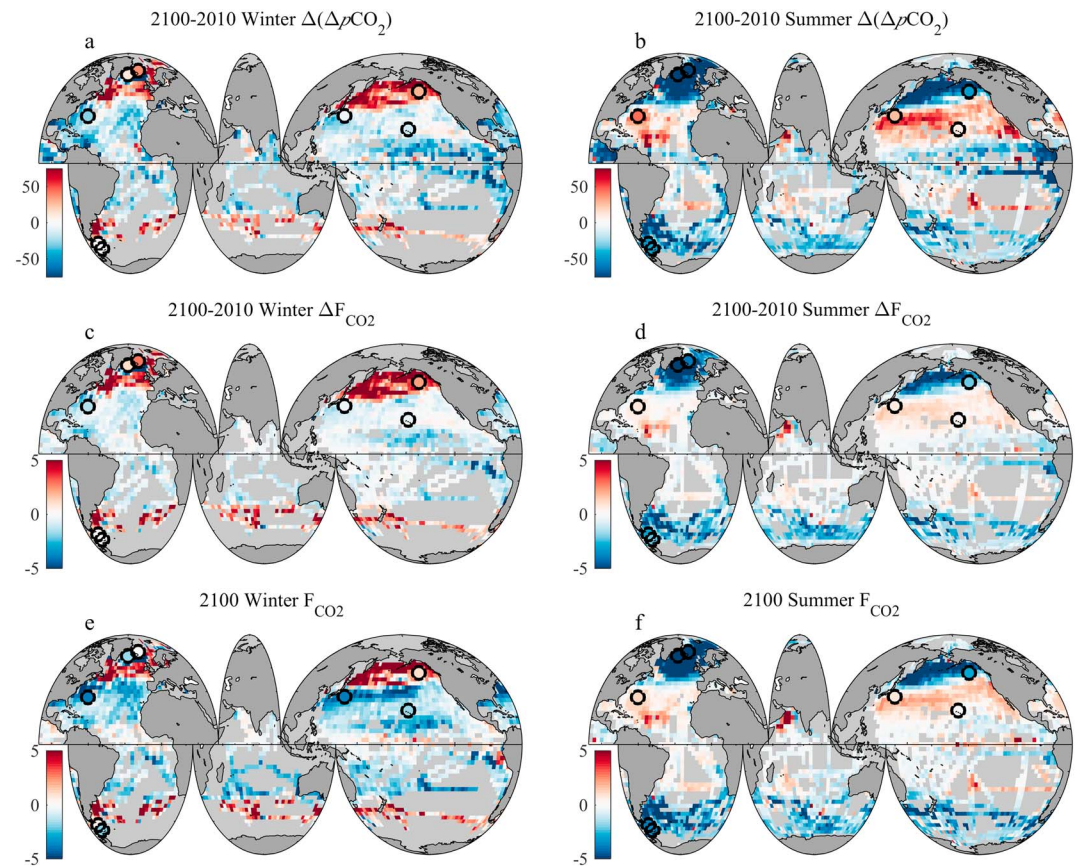
Figure 10. Changes in winter and summer (a–b) $\Delta p CO_{2\ Sea-Air}$ (µatm) and (c–d) sea-air CO_2 flux (F_{CO2}; g C m^{-2} mo^{-1}) from 2010 to 2100. Winter (summer) is defined as January through March in the northern (southern) hemisphere and July through September in the southern (northern) hemisphere. (e) 2100 winter and (f) summer sea-air CO_2 flux (F_{CO2}; g C m^{-2} mo^{-1}). Data are plotted for SOCAT-v4 grids with at least 4 months of the climatology represented. Circles show select time series and are colored independently of the maps. In panels (a)–(d), red indicates a reduced sink or enhanced source and blue indicates an enhanced sink or reduced source. SOCAT-v4 = Surface Ocean CO_2 Atlas version 4.

known seasonal drivers of $p CO_2$ variability (Figure 1a). On the other hand, winter F_{CO2} changes are slightly larger than the summer F_{CO2} changes due to differences in the magnitude and pattern of seasonal wind speed (Figure S11). Changes in the winter F_{CO2} suggest reduced ocean carbon uptake in the northern hemisphere high latitudes and increased carbon uptake in the temperate and tropical regions over this time period. During summer, there is slightly enhanced ocean carbon uptake in the high latitudes. These results match what was found for the time series sites (Figure 7) though the Southern Ocean is poorly characterized during winter, making it infeasible to determine whether the time series site results are zonally representative. Notably, the flux changes relative to 1861 are nonnegligible when compared to modern (2010) sea-air fluxes (Figures 9e and 9f), suggesting the potential for carbonate chemistry to have influenced CO_2 fluxes since 1861, in the absence of changes to other processes. Additionally, the pattern of change indicates that the 1861 drivers of seasonal $p CO_2$ variations were largely maintained or strengthened through 2010 (Figure S8).

Figure 10 is the same as Figure 9 but for the 2010 to 2100 time period. $\Delta p CO_{2\ Sea-Air}$ increases (decreases) in the high latitudes during winter (summer) and in the subtropical gyres during summer (winter). These results agree with the time series site findings (Figure 7) and again suggest that the pattern of processes controlling seasonal $p CO_2$ variations is generally maintained (Figure S8). Changes in F_{CO2} from 2010 to 2100 during both seasons are much larger than the 1861 to 2010 changes, reflecting larger seasonal differences between air and sea $p CO_2$ values over this time. Since all components of the flux calculation are derived from climatologies excluding the small model transient components for SSS, SST, and TA, this result largely reflects the chemical thermodynamic response to rising DIC under the RCP8.5 concentration pathway. Further, the F_{CO2}
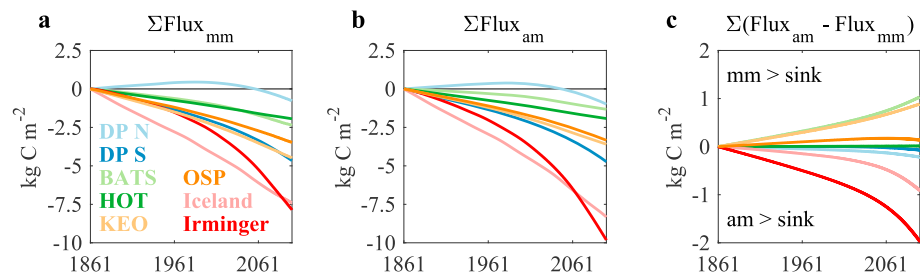
Figure 11. Cumulative monthly sea-air CO_2 flux determined using (a) monthly mean (mm) and (b) annual mean (am) values for ΔpCO_2 $_{Sea-Air}$. (c) Difference between the annual and monthly mean cumulative fluxes.

changes are largest in the high latitudes and comparable in magnitude to the 2010 fluxes (Figures 9e and 9f), exhibiting a similar spatial pattern. This leads to an enhancement of the seasonal flux magnitude in most locations by 2100, as shown in Figures 10e and 10f. Larger magnitude ΔpCO_2 $_{Sea-Air}$ (and F_{CO2}) changes at the high latitudes relative to the subtropics reflect more rapid growth in RF (Fassbender, Sabine, & Palevsky, 2017), which works to amplify the efficiency at which seasonal DIC changes modulate pCO_2 (Figures 2f and S10b; Hauck & Völker, 2015). Additionally, amplification of the RF seasonal cycle allows pCO_2 $_{BP}$ to display increasingly nonlinear characteristics that work to outpace or catch up to the linear (with respect to pCO_2 $_{am}$) pCO_2 $_T$ seasonal cycle growth over time (Figures 8i–8l). This is likely why seasonal changes in pCO_2 and F_{CO2} are muted in the subtropical gyres relative to the high latitudes through 2100.

In light of seasonal asymmetries in the response of sea surface pCO_2 to its various drivers under anthropogenic carbon accumulation, it may be important to consider the resulting influence on CO_2 fluxes computed from annual mean pCO_2 values. This is particularly relevant as the flux seasonality is not only a function of ΔpCO_2 $_{Sea-Air}$ but also of wind speed (Wanninkhof, 2014), which can amplify seasonal ΔpCO_2 $_{Sea-Air}$ differences (e.g., Figures 7c and 7f). To test the importance of resolving seasonal pCO_2 variations for sea-air flux assessments, we calculate the cumulative monthly sea-air CO_2 flux at each time series site from 1861 to 2100 using the monthly resolved ΔpCO_2 $_{Sea-Air}$ and the annual mean ΔpCO_2 $_{Sea-Air}$. The results are shown in Figure 11 where a range of responses are found across all time series sites, with differences as large as ~25% in the monthly resolved versus annual mean computed cumulative fluxes by 2100. This suggests that resolving the monthly sea-air disequilibrium is necessary to accurately quantify regional, and possibly global, CO_2 fluxes due to seasonal asymmetries in ΔpCO_2 $_{Sea-Air}$ that evolve under anthropogenic carbon invasion into the ocean.

6. Conclusions

Our main objective was to develop an observationally anchored framework for understanding how seasonal variations in the surface ocean carbon cycle will respond to the invasion of anthropogenic carbon through 2100. Our approach combines a climatology (corresponding to the year 2010) of carbon cycle-pertinent variables derived from an observational data product with a model representation of the anthropogenic DIC increase (annual mean) over 1861–2100 (with minimum adjustments from other variables as appropriate). In choosing model output from the BGC configuration of GFDL's ESM2M, we purposefully isolated ocean biogeochemistry changes caused by the full evolution of historical/RCP8.5 atmospheric CO_2 while maintaining the preindustrial radiative balance in the atmosphere (i.e., no anthropogenically induced warming). With this hybrid representation of the anthropogenic CO_2 in the ocean, our explicit goal was to build on the previous study of Hauck and Völker (2015) and test the hypothesis that there are important asymmetries in the seasonal cycle responses of surface ocean carbon chemistry variables to the invasion of anthropogenic CO_2.

We find that modern surface ocean pCO_2 seasonal cycles result from a combination of seasonal SST and DIC variations as well as regional chemical conditions (annual mean pCO_2 and RF). Spatial heterogeneity in temperature driven pCO_2 seasonal cycles may simply reflect differences in the annual mean pCO_2 rather than the SST range. Similarly, larger spring and summer pCO_2 drawdown in one region does not necessarily equate to higher biological productivity, as it may reflect a lower buffer capacity (higher RF) and more efficient manipulation of pCO_2 by biophysical processes. This finding alone hints that the entrainment and subsequent

export of equal amounts of carbon and nutrients does not yield the same $p\text{CO}_2$ response in all locations. Instead, the RF modulates the influence of DIC on $p\text{CO}_2$ and, thus, the uptake of atmospheric carbon, both spatially as well as over time, in the absence of differences in or changes to biological processes and ocean mixing. This finding may revive a historical debate on the topic that was fittingly instigated by Roger Revelle (Broecker, 1991; Longhurst, 1991; Revelle, 1990, 1991; Sarmiento, 1991; Smith & Mackenzie, 1991). Seasonal $p\text{CO}_2$ characteristics directly influence seawater acidity ($[\text{H}^+]$), and our findings show that the seasonal cycle amplitude (A) of $p\text{CO}_2$ and $[\text{H}^+]$ will likely grow or be maintained in all ocean regions as ocean carbon content rises, though this result is sensitive to the evaluation timescale (see section 5). In contrast, A-pH may be expected to decline in the subtropics due to faster growth in the annual mean $[\text{H}^+]$ than in A-$[\text{H}^+]$. In light of these confounding pH characteristics, it may be useful to evaluate regional acidity changes in terms of $[\text{H}^+]$ rather than pH to ensure accurate interpretations of ocean acidification.

The central result of this study is the identification of a potentially important asymmetry in the response of the surface ocean carbon cycle over the 21st century. This is caused by linear amplification of the thermal component of seasonal $p\text{CO}_2$ variations and nonlinear amplification of the biophysical component of seasonal $p\text{CO}_2$ variations. Because these competing modes of seasonal variability exhibit spatially nonuniform and unique amplification characteristics, seasonal $p\text{CO}_2$ cycles are subject to significant changes. This includes more than a doubling in magnitude in some cases (e.g., Figures 3a–3d and 4f), as well as complete phase shifts in seasonality near gyre boundary regions. Nonlinearity in how biophysical processes influence seasonal $p\text{CO}_2$ variations over time is caused by nonlinear growth in the RF, which magnifies the sensitivity of $p\text{CO}_2$ to perturbations in DIC. Further, this effect is seasonally asymmetric due to seasonality in the RF and amplification of this seasonality over time (Figure S10a). Thus, the $p\text{CO}_2$ seasonal cycle response projects onto the RF perturbations resulting from anthropogenic carbon invasion into the ocean, which has potentially important implications for our understanding of carbon-climate feedbacks (Revelle & Suess, 1957). It is our intention that this result informs further efforts to understand the role of the RF in sustaining positive carbon-climate feedbacks, as the mechanism identified herein is not presently accounted for in the feedback analysis methodology of Friedlingstein et al. (2003) and Friedlingstein et al. (2006).

For understanding climate perturbations in a linear framework, the moniker "mean state" typically denotes a stationary basic state that exhibits small perturbations. Within a mean state framework, timescales of variability (preindustrial state, seasonal cycle, natural variability, and secular trend) are assumed to be independent and separable. Our identification of an asymmetric response in seasonal variations of the surface ocean carbon cycle under continued anthropogenic carbon emissions defies this construct. We find that seasonal variability is not only amplified by ongoing changes associated with the secular trend, but that alteration of the seasonal cycle can in turn impact the magnitude of the secular trend. Thus, the annual or decadal mean carbonate system state (considered as a time-average) will rarely (if ever) reflect the instantaneous state of the system due to underlying nonlinearities in the seasonal cycle of the carbonate system itself.

Asymmetric amplification of the $p\text{CO}_2$ seasonality thus challenges our ability to use annual mean sea surface $p\text{CO}_2$ values to accurately quantify ocean CO_2 uptake over time, as the annual mean $p\text{CO}_2$ becomes progressively less representative of $p\text{CO}_2$ values during the dominant flux season (often winter). These asymmetries, where seasonal minimums change at a different rate than seasonal maximums, highlight ongoing challenges with using a summer-biased observing network (particularly in the Southern Ocean, see Figure 1 in Williams et al., 2017) to characterize anthropogenic trends, as different seasons will exhibit different rates of change. Our findings also suggest that models will need to accurately reproduce observed $p\text{CO}_2$ seasonal cycles (not just annual means) in order to improve confidence in future projections of ocean carbon uptake (see recent discussion by Goris et al., 2018). Of course, the ultimate evolution of $p\text{CO}_2$ seasonal cycles will depend on more than just the natural and anthropogenic carbon cycle interactions considered here, as changes in seasonal SST and DIC dynamics as well as other ocean processes will play an important role. For example, rising temperatures will result in higher annual mean sea surface $p\text{CO}_2$ values as CO_2 becomes less soluble, which will lend more leverage to thermal drivers of seasonal $p\text{CO}_2$ variations (equation (2)). Changes in the ocean physical state, such as increased stratification or modified wind mixing, may impact the seasonal range in DIC, TA, RF, SST, and SSS. Changes to biological carbon production caused by altered ecosystem structure, shifting nutrient uptake ratios, or the impacts of ocean acidification could also result in modified seasonal DIC and TA variations. Thus, it is important to reiterate that our work aims to characterize the chemical response

of the carbonate system in isolation so that it can be incorporated into the interpretation of marine carbon cycle changes found in observations and fully coupled models.

In closing, it is often assumed that the biological pump has remained constant since the preindustrial period and that anthropogenic carbon merely imprints on top of the natural background. This assumption stems from our present inability to tightly constrain modern biological carbon export in the ocean (Siegel et al., 2016). However, it is plausible that the biological pump is not in steady state, and numerous carbon cycle feedbacks related to the biological pump have been identified (e.g., Falkowski, 1998; Passow & Carlson, 2012). How then does the research community differentiate natural and anthropogenic biochemical signatures of carbon cycling (e.g., air-sea $p\text{CO}_2$ disequilibrium) when amplification processes may already be entangled with a shifting baseline? This question requires careful community reflection as it may necessitate a refinement of the methods commonly used to separate natural and anthropogenic carbon cycles.

References

Anav, A., Friedlingstein, P., Kidston, M., Bopp, L., Ciais, P., Cox, P., et al. (2013). Evaluating the land and ocean components of the global carbon cycle in the CMIP5 earth system models. *Journal of Climate*, 26(18), 6801–6843. https://doi.org/10.1175/JCLI-D-12-00417.1

Arora, V. K., Boer, G. J., Friedlingstein, P., Eby, M., Jones, C. D., Christian, J. R., et al. (2013). Carbon-concentration and carbon-climate feedbacks in CMIP5 earth system models. *Journal of Climate*, 26(15), 5289–5314. https://doi.org/10.1175/JCLI-D-12-00494.1

Bakker, D. C. E., Pfeil, B., Landa, C. S., Metzl, N., O'Brien, K. M., Olsen, A., et al. (2016). A multi-decade record of high-quality *f*CO$_2$ data in version 3 of the Surface Ocean CO$_2$ Atlas (SOCAT) Dorothee. *Earth System Science Data*, 8(2), 383–413. https://doi.org/10.5194/essd-8-383-2016

Bates, N., Astor, Y., Church, M. J., Currie, K., Dore, J., Gonaález-Dávila, M., et al. (2014). A time-series view of changing ocean chemistry due to ocean uptake of anthropogenic CO$_2$ and ocean acidification. *Oceanography*, 27(1), 126–141. https://doi.org/10.5670/oceanog.2014.16

Broecker, W. S. (1991). Keeping global change honest. *Global Biogeochemical Cycles*, 5(3), 191–192. https://doi.org/10.1029/91GB01421

Broecker, W. S., Takahashi, T., Simpson, H. J., & Peng, T.-H. (1979). Fate of fossil fuel carbon dioxide and the global carbon budget. *Science (New York, N.Y.)*, 206(4417), 409–418. https://doi.org/10.1126/science.206.4417.409

Cai, W.-J., Hu, X., Huang, W.-J., Murrell, M. C., Lehrter, J. C., Lohrenz, S. E., et al. (2011). Acidification of subsurface coastal waters enhanced by eutrophication. *Nature Geoscience*, 4(11), 766–770. https://doi.org/10.1038/ngeo1297

Carter, B. R., Williams, N. L., Gray, A. R., & Feely, R. A. (2016). Locally interpolated alkalinity regression for global alkalinity estimation. *Limnology and Oceanography: Methods*, 14(4), 268–277. https://doi.org/10.1002/lom3.10087

Dee, D. P., Uppala, S. M., Simmons, A. J., Berrisford, P., Poli, P., Kobayashi, S., et al. (2011). The ERA-Interim reanalysis: Configuration and performance of the data assimilation system. *Quarterly Journal of the Royal Meteorological Society*, 137(656), 553–597. https://doi.org/10.1002/qj.828

Dickson, A. G. (1990). Standard potential of the reaction: AgCl(s) + 1/2H$_2$(g) = Ag(s) + HCl (aq), and the standard acidity constant of the ion HSO$_4^-$ in synthetic sea water from 273.15 to 318.15 K. *The Journal of Chemical Thermodynamics*, 22(2), 113–127. https://doi.org/10.1016/0021-9614(90)90074-Z

Dunne, J. P., John, J. G., Adcroft, A. J., Griffies, S. M., Hallberg, R. W., Shevliakova, E., et al. (2012). GFDL's ESM 2 global coupled climate-carbon earth system models. Part I: Physical formulation and baseline simulation characteristics. *Journal of Climate*, 25(19), 6646–6665. https://doi.org/10.1175/JCLI-D-11-00560.1

Dunne, J. P., John, J. G., Shevliakova, E., Stouffer, R. J., Krasting, J. P., Malyshev, S. L., et al. (2013). GFDL's ESM 2 global coupled climate-carbon earth system models. Part II: Carbon system formulation and baseline simulation characteristics. *Journal of Climate*, 26(7), 2247–2267. https://doi.org/10.1175/JCLI-D-12-00150.1

Egleston, E. S., Sabine, C. L., & Morel, F. M. M. (2010). Revelle revisited: Buffer factors that quantify the response of ocean chemistry to changes in DIC and alkalinity. *Global Biogeochemical Cycles*, 24, GB1002. https://doi.org/10.1029/2008GB003407

Falkowski, P. G. (1998). Biogeochemical controls and feedbacks on ocean primary production. *Science*, 281(5374), 200–206. https://doi.org/10.1126/science.281.5374.200

Fassbender, A. J., Sabine, C. L., & Cronin, M. F. (2016). Net community production and calcification from 7 years of NOAA Station Papa Mooring measurements. *Global Biogeochemical Cycles*, 30, 250–267. https://doi.org/10.1002/2015GB005205

Fassbender, A. J., Sabine, C. L., Cronin, M. F., & Sutton, A. J. (2017). Mixed-layer carbon cycling at the Kuroshio Extension Observatory. *Global Biogeochemical Cycles*, 31, 272–288. https://doi.org/10.1002/2016GB005547

Fassbender, A. J., Sabine, C. L., & Palevsky, H. I. (2017). Nonuniform ocean acidification and attenuation of the ocean carbon sink. *Geophysical Research Letters*, 44, 8404–8413. https://doi.org/10.1002/2017GL074389

Fay, A. R., & McKinley, G. A. (2013). Global trends in surface ocean *p*CO$_2$ from in situ data. *Global Biogeochemical Cycles*, 27, 541–557. https://doi.org/10.1002/gbc.20051

Frankignoulle, M. (1994). A complete set of buffer factors for acid/base CO$_2$ system in seawater. *Journal of Marine Systems*, 5(2), 111–118. https://doi.org/10.1016/0924-7963(94)90026-4

Frankignoulle, M., Canon, C., & Gattuso, J.-P. (1994). Marine calcification as a source of carbon dioxide: Positive feedback of increasing atmospheric CO$_2$. *Limnology and Oceanography*, 39(2), 458–462. https://doi.org/10.4319/lo.1994.39.2.0458

Friedlingstein, P., Cox, P., Betts, R., Bopp, L., von Bloh, W., Brovkin, V., et al. (2006). Climate–carbon cycle feedback analysis: Results from the C4MIP Model Intercomparison. *Journal of Climate*, 19(14), 3337–3353. https://doi.org/10.1175/JCLI3800.1

Friedlingstein, P., Dufresne, J.-L., Cox, P. M., & Rayner, P. (2003). How positive is the feedback between climate change and the carbon cycle? *Tellus B*, 55(2), 692–700. https://doi.org/10.1034/j.1600-0889.2003.01461.x

González-Dávila, M., Santana-Casiano, J. M., Rueda, M. J., & Llinas, O. (2010). The water column distribution of carbonate system variables at the ESTOC site from 1995 to 2004. *Biogeosciences*, 7(10), 3067–3081. https://doi.org/10.5194/bg-7-3067-2010

Gorgues, T., Aumont, O., & Rodgers, K. B. (2010). A mechanistic account of increasing seasonal variations in the rate of ocean uptake of anthropogenic carbon. *Biogeosciences*, 7(8), 2581–2589. https://doi.org/10.5194/bg-7-2581-2010

Goris, N., Tjiputra, J. F., Olsen, A., Schwinger, J., Lauvset, S. K., & Jeansson, E. (2018). Constraining projection-based estimates of the future North Atlantic carbon uptake. *Journal of Climate*, 31(10), 3959–3978. https://doi.org/10.1175/JCLI-D-17-0564.1

Gregory, J. M., Jones, C. D., Cadule, P., & Friedlingstein, P. (2009). Quantifying carbon cycle feedbacks. *Journal of Climate*, *22*(19), 5232–5250. https://doi.org/10.1175/2009JCLI2949.1

Hagens, M., & Middelburg, J. J. (2016). Attributing seasonal pH variability in surface ocean waters to governing factors. *Geophysical Research Letters*, *43*, 12,528–12,537. https://doi.org/10.1002/2016GL071719

Hagens, M., Slomp, C. P., Meysman, F. J. R., Seitaj, D., Harlay, J., Borges, A. V., et al. (2015). Biogeochemical processes and buffering capacity concurrently affect acidification in a seasonally hypoxic coastal marine basin. *Biogeosciences*, *12*, 1561–1583. https://doi.org/10.5194/bg-12-1561-2015

Hall, A., & Qu, X. (2006). Using the current seasonal cycle to constrain snow albedo feedback in future climate change. *Geophysical Research Letters*, *33*, L03502. https://doi.org/10.1029/2005GL025127

Hall, T. M., Waugh, D. W., Haine, T. W. N. N., Robbins, P. E., & Khatiwala, S. (2004). Estimates of anthropogenic carbon in the Indian Ocean with allowance for mixing and time-varying air-sea CO_2 disequilibrium. *Global Biogeochemical Cycles*, *18*, GB1031. https://doi.org/10.1029/2003GB002120

Hauck, J., & Völker, C. (2015). Rising atmospheric CO_2 leads to large impact of biology on Southern Ocean CO_2 uptake via changes of the Revelle factor. *Geophysical Research Letters*, *42*, 1459–1464. https://doi.org/10.1002/2015GL063070.1

Hauck, J., Völker, C., Wolf-Gladrow, D. A., Laufkötter, C., Vogt, M., Aumont, O., et al. (2015). On the Southern Ocean CO_2 uptake and the role of the biological carbon pump in the 21st century. *Global Biogeochemical Cycles*, *29*, 1451–1470. https://doi.org/10.1002/2015GB005140

Ilyina, T. (2016). Climate science: Hidden trends in the ocean carbon sink. *Nature*, *530*(7591), 426–427. https://doi.org/10.1038/530426a

Körtzinger, A., Send, U., Lampitt, R. S., Hartman, S., Wallace, D. W. R., Karstensen, J., et al. (2008). The seasonal pCO_2 cycle at 49°N/16.5°W in the northeastern Atlantic Ocean and what it tells us about biological productivity. *Journal of Geophysical Research*, *113*, C04020. https://doi.org/10.1029/2007JC004347

Kwiatkowski, L., Bopp, L., Aumont, O., Ciais, P., Cox, P. M., Laufkötter, C., et al. (2017). Emergent constraints on projections of declining primary production in the tropical oceans. *Nature Climate Change*, *7*(5), 355–358. https://doi.org/10.1038/nclimate3265

Kwiatkowski, L., & Orr, J. C. (2018). Diverging seasonal extremes for ocean acidification during the twenty-first century. *Nature Climate Change*, *8*(2), 141–145. https://doi.org/10.1038/s41558-017-0054-0

Landschützer, P., Gruber, N., & Bakker, D. C. E. (2016). Decadal variations and trends of the global ocean carbon sink. *Global Biogeochemical Cycles*, *30*, 1396–1417. https://doi.org/10.1002/2015GB005359

Landschützer, P., Gruber, N., Bakker, D. C. E., & Schuster, U. (2014). Recent variability of the global ocean carbon sink. *Global Biogeochemical Cycles*, *28*, 927–949. https://doi.org/10.1002/2014GB004853

Landschützer, P., Gruber, N., Bakker, D. C. E., Stemmler, I., & Six, K. D. (2018). Strengthening seasonal marine CO_2 variations due to increasing atmospheric CO_2. *Nature Climate Change*, *8*(2), 146–150. https://doi.org/10.1038/s41558-017-0057-x

Lauvset, S. K., Gruber, N., Landschützer, P., Olsen, A., & Tjiputra, J. (2015). Trends and drivers in global surface ocean pH over the past 3 decades. *Biogeosciences*, *12*(5), 1285–1298. https://doi.org/10.5194/bg-12-1285-2015

Le Quéré, C., Andrew, R. M., Canadell, J. G., Sitch, S., Korsbakken, J. I., Peters, G. P., et al. (2016). Global carbon budget 2016. *Earth System Science Data*, *8*(2), 605–649. https://doi.org/10.5194/essd-8-605-2016

Le Quéré, C., Andrew, R. M., Friedlingstein, P., Sitch, S., Pongratz, J., Manning, A. C., et al. (2018). Global carbon budget 2017. *Earth System Science Data Discussions*, 1–79. https://doi.org/10.5194/essd-2017-123

Le Quéré, C., Moriarty, R., Andrew, R. M., Canadell, J. G., Sitch, S., Korsbakken, J. I., et al. (2015). Global carbon budget 2017. *Earth System Science Data*, *10*(1), 405–448. https://doi.org/10.5194/essd-10-405-2018

Le Quéré, C., Rodenbeck, C., Buitenhuis, E. T., Conway, T. J., Langenfelds, R., Gomez, A., et al. (2007). Saturation of the Southern Ocean CO_2 sink due to recent climate change. *Science*, *316*(5832), 1735–1738. https://doi.org/10.1126/science.1136188

Lenton, A., & Matear, R. J. (2007). Role of the Southern Annular Mode (SAM) in Southern Ocean CO_2 uptake. *Global Biogeochemical Cycles*, *21*, GB2016. https://doi.org/10.1029/2006GB002714

Lenton, A., Metzl, N., Takahashi, T., Kuchinke, M., Matear, R. J., Roy, T., et al. (2012). The observed evolution of oceanic pCO_2 and its drivers over the last two decades. *Global Biogeochemical Cycles*, *26*, GB2021. https://doi.org/10.1029/2011GB004095

Lewis, E., & Wallace, D. W. (1998). *Program developed for CO_2 system calculations*, (Vol. 4735). Oak Ridge TN: Oak Ridge National Laboratory Environmental Sciences Division. Retrieved from http://cdiac.ornl.gov/ftp/co2sys/CO2SYS_calc_DOS_v1.05/co2sys_v1.05.txt

Longhurst, A. R. (1991). A reply to Broecker's charges. *Global Biogeochemical Cycles*, *5*(4), 315–316. https://doi.org/10.1029/91GB02738

Lovenduski, N. S., Gruber, N., Doney, S. C., & Lima, I. D. (2007). Enhanced CO_2 outgassing in the Southern Ocean from a positive phase of the Southern Annular Mode. *Global Biogeochemical Cycles*, *21*, GB2026. https://doi.org/10.1029/2006GB002900

Lovenduski, N. S., Long, M. C., & Lindsay, K. (2015). Natural variability in the surface ocean carbonate ion concentration. *Biogeosciences*, *12*(21), 6321–6335. https://doi.org/10.5194/bg-12-6321-2015

Lueker, T. J., Dickson, A. G., & Keeling, C. D. (2000). Ocean pCO_2 calculated from dissolved inorganic carbon, alkalinity, and equations for K_1 and K_2: Validation based on laboratory measurements of CO_2 in gas and seawater at equilibrium. *Marine Chemistry*, *70*(1–3), 105–119. https://doi.org/10.1016/S0304-4203(00)00022-0

Matsumoto, K., & Gruber, N. (2005). How accurate is the estimation of anthropogenic carbon in the ocean? An evaluation of the ΔC^* method. *Global Biogeochemical Cycles*, *19*, GB3014. https://doi.org/10.1029/2004GB002397

McKinley, G. A., Fay, A. R., Lovenduski, N. S., & Pilcher, D. J. (2017). Natural variability and anthropogenic trends in the ocean carbon sink. *Annual Review of Marine Science*, *9*(1), 125–150. https://doi.org/10.1146/annurev-marine-010816-060529

McKinley, G. A., Pilcher, D. J., Fay, A. R., Lindsay, K., Long, M. C., & Lovenduski, N. S. (2016). Timescales for detection of trends in the ocean carbon sink. *Nature*, *530*(7591), 469–472. https://doi.org/10.1038/nature16958

McKinley, G. A., Takahashi, T., Buitenhuis, E. T., Chai, F., Christian, J. R., Doney, S. C., et al. (2006). North Pacific carbon cycle response to climate variability on seasonal to decadal timescales. *Journal of Geophysical Research*, *111*, C07S06. https://doi.org/10.1029/2005JC003173

McNeil, B. I., & Sasse, T. P. (2016). Future ocean hypercapnia driven by anthropogenic amplification of the natural CO_2 cycle. *Nature*, *529*(7586), 383–386. https://doi.org/10.1038/nature16156

Moss, R. H., Edmonds, J. A., Hibbard, K. A., Manning, M. R., Rose, S. K., van Vuuren, D. P., et al. (2010). The next generation of scenarios for climate change research and assessment. *Nature*, *463*(7282), 747–756. https://doi.org/10.1038/nature08823

Munro, D. R., Lovenduski, N. S., Takahashi, T., Stephens, B. B., Newberger, T., & Sweeney, C. (2015). Recent evidence for a strengthening CO_2 sink in the Southern Ocean from carbonate system measurements in the Drake Passage (2002-2015). *Geophysical Research Letters*, *42*, 7623–7630. https://doi.org/10.1002/2015GL065194

Nakano, H., Tsujino, H., Hirabara, M., Yasuda, T., Motoi, T., Ishii, M., et al. (2011). Uptake mechanism of anthropogenic CO_2 in the Kuroshio Extension region in an ocean general circulation model. *Journal of Oceanography*, *67*(6), 765–783. https://doi.org/10.1007/s10872-011-0075-7

Olafsson, J., Olafsdottir, S. R., Benoit-Cattin, A., Danielsen, M., Arnarson, T. S., & Takahashi, T. (2009). Rate of Iceland Sea acidification from time series measurements. *Biogeosciences Discussions*, 6(3), 5251–5270. https://doi.org/10.5194/bgd-6-5251-2009

Orr, J. C., Epitalon, J.-M., & Gattuso, J.-P. (2015). Comparison of ten packages that compute ocean carbonate chemistry. *Biogeosciences*, 12(5), 1483–1510. https://doi.org/10.5194/bg-12-1483-2015

Pacella, S. R., Brown, C. A., Waldbusser, G. G., Labiosa, R. G., & Hales, B. (2018). Seagrass habitat metabolism increases short-term extremes and long-term offset of CO_2 under future ocean acidification. *Proceedings of the National Academy of Sciences*, 115(15), 3870–3875. https://doi.org/10.1073/pnas.1703445115

Passow, U., & Carlson, C. A. (2012). The biological pump in a high CO_2 world. *Marine Ecology Progress Series*, 470(2), 249–271. https://doi.org/10.3354/meps09985

Revelle, R. (1990). Letter in forum section. *Issues in Science and Technology*, 7(2), 21–22.

Revelle, R. (1991). Response to the comment by S.V. Smith and F.T. Mackenzie. *Global Biogeochemical Cycles*, 5(4), 317–317. https://doi.org/10.1029/91GB02737

Revelle, R., & Suess, H. E. (1957). Carbon dioxide exchange between atmosphere and ocean and the question of an increase of atmospheric CO_2 during the past decades. *Tellus*, 9(1), 18–27. https://doi.org/10.1111/j.2153-3490.1957.tb01849.x

Riebesell, U., Körtzinger, A., & Oschlies, A. (2009). Sensitivities of marine carbon fluxes to ocean change. *Proceedings of the National Academy of Sciences*, 106(49), 20602–20609. https://doi.org/10.1073/pnas.0813291106

Rodgers, K. B., Sarmiento, J. L., Aumont, O., Crevoisier, C., de Boyer Montégut, C., & Metzl, N. (2008). A wintertime uptake window for anthropogenic CO_2 in the North Pacific. *Global Biogeochemical Cycles*, 22, GB2020. https://doi.org/10.1029/2006GB002920

Sabine, C. L., Feely, R. A., Gruber, N., Key, R. M., Lee, K., Bullister, J. L., et al. (2004). The oceanic sink for anthropogenic CO_2. *Science*, 305(5682), 367–371. https://doi.org/10.1126/science.1097403

Sarmiento, J. L. (1991). Oceanic uptake of anthropogenic CO_2: The major uncertainties. *Global Biogeochemical Cycles*, 5(4), 309–313. https://doi.org/10.1029/91GB02705

Sarmiento, J. L., & Gruber, N. (2006). Carbon cycle. In *Ocean biogeochemical dynamics* (pp. 318–355). New Jersey: Princeton University Press.

Sasse, T. P., McNeil, B. I., Matear, R. J., & Lenton, A. (2015). Quantifying the influence of CO_2 seasonality on future aragonite undersaturation onset. *Biogeosciences*, 12(20), 6017–6031. https://doi.org/10.5194/bg-12-6017-2015

Schwinger, J., Tjiputra, J. F., Heinze, C., Bopp, L., Christian, J. R., Gehlen, M., et al. (2014). Nonlinearity of ocean carbon cycle feedbacks in CMIP5 earth system models. *Journal of Climate*, 27(11), 3869–3888. https://doi.org/10.1175/JCLI-D-13-00452.1

Shaw, E. C., McNeil, B. I., Tilbrook, B., Matear, R., & Bates, M. L. (2013). Anthropogenic changes to seawater buffer capacity combined with natural reef metabolism induce extreme future coral reef CO2 conditions. *Global Change Biology*, 19(5), 1632–1641. https://doi.org/10.1111/gcb.12154

Siegel, D. A., Buesseler, K. O., Behrenfeld, M. J., Benitez-Nelson, C. R., Boss, E., Brzezinski, M. A., et al. (2016). Prediction of the export and fate of global ocean net primary production: The EXPORTS Science Plan. *Frontiers in Marine Science*, 3(March), 1–10. https://doi.org/10.3389/fmars.2016.00022

Smith, S. V., & Mackenzie, F. T. (1991). Comments on the role of oceanic biota as a sink for anthropogenic CO_2 emissions. *Global Biogeochemical Cycles*, 5(3), 189–190. https://doi.org/10.1029/91GB01384

Sundquist, E. T., Plummer, L. N., & Wigley, T. M. L. (1979). Carbon dioxide in the ocean surface: The homogeneous buffer factor. *Science*, 204(4398), 1203–1205. https://doi.org/10.1126/science.204.4398.1203

Sutton, A. J., Feely, R. A., Sabine, C. L., McPhaden, M. J., Takahashi, T., Chavez, F. P., et al. (2014). Natural variability and anthropogenic change in equatorial Pacific surface ocean $p$$CO_2$ and pH. *Global Biogeochemical Cycles*, 28, 131–145. https://doi.org/10.1002/2013GB004679

Takahashi, T., Broecker, W. S., Werner, S. R., & Bainbridge, A. E. (1980). Carbonate chemistry of the surface waters of the worlds ocean. In E. D. Goldberg, Y. Horibe, & K. Saruhashi (Eds.), *Isotope marine chemistry* (pp. 291–326). Tokyo: Published for Geochemistry Research Association by Uchida Rokakuho Pub. Co.

Takahashi, T., Olafsson, J., Goddard, J. G., Chipman, D. W., & Sutherland, S. C. (1993). Seasonal variation of CO_2 and nutrients in the high-latitude surface oceans: A comparative study. *Global Biogeochemical Cycles*, 7(4), 843–878. https://doi.org/10.1029/93GB02263

Takahashi, T., Sutherland, S. C., Chipman, D. W., Goddard, J. G., & Ho, C. (2014). Climatological distributions of pH, $p$$CO_2$, total CO_2, alkalinity, and $CaCO_3$ saturation in the global surface ocean, and temporal changes at selected locations. *Marine Chemistry*, 164, 95–125. https://doi.org/10.1016/j.marchem.2014.06.004

Takahashi, T., Sutherland, S. C., Sweeney, C., Poisson, A., Metzl, N., Tilbrook, B., et al. (2002). Global sea–air CO_2 flux based on climatological surface ocean $p$$CO_2$, and seasonal biological and temperature effects. *Deep Sea Research Part II: Topical Studies in Oceanography*, 49(9–10), 1601–1622. https://doi.org/10.1016/S0967-0645(02)00003-6

Takahashi, T., Sutherland, S. C., Wanninkhof, R., Sweeney, C., Feely, R. A., Chipman, D. W., et al. (2009). Climatological mean and decadal change in surface ocean $p$$CO_2$, and net sea-air CO_2, flux over the global oceans. *Deep Sea Research, Part II*, 56(8–10), 554–577. https://doi.org/10.1016/j.dsr2.2008.12.009

Thomas, H., Friederike Prowe, A. E., van Heuven, S. M. A. C., Bozec, Y., de Baar, H. J. W., Schiettecatte, L.-S., et al. (2007). Rapid decline of the CO_2 buffering capacity in the North Sea and implications for the North Atlantic Ocean. *Global Biogeochemical Cycles*, 21, GB4001. https://doi.org/10.1029/2006GB002825

Uppström, L. R. (1974). The boron-chlorinity ratio of deep seawater from the Pacific Ocean. *Deep-Sea Research Part I*, 21, 161–162.

van Heuven, S. M. A. C., Pierrot, D., Rae, J. W. B., Lewis, E., & Wallace, D. W. (2011). MATLAB program developed for CO_2 system calculations. ORNL/CDIAC-105b. *ORNL/CDIAC-105b. Carbon Dioxide Information Analysis Center, Oak Ridge National Laboratory, U.S. Department of Energy, Oak Ridge, Tennessee*. doi: 10.3334/CDIAC/otg.CO2SYS_MATLAB_v1.1

van Vuuren, D. P., Edmonds, J., Kainuma, M., Riahi, K., Thomson, A., Hibbard, K., et al. (2011). The representative concentration pathways: An overview. *Climatic Change*, 109(1–2), 5–31. https://doi.org/10.1007/s10584-011-0148-z

Wanninkhof, R. (1992). Relationship between wind speed and gas exchange over the ocean. *Journal of Geophysical Research*, 97(C5), 7373–7382. https://doi.org/10.1029/92JC00188

Wanninkhof, R. (2014). Relationship between wind speed and gas exchange over the ocean revisited. *Limnology and Oceanography: Methods*, 12(6), 351–362. https://doi.org/10.4319/lom.2014.12.351

Wanninkhof, R., Park, G. H.-H. H., Takahashi, T., Sweeney, C., Feely, R. A., Nojiri, Y., et al. (2013). Global ocean carbon uptake: Magnitude, variability and trends. *Biogeosciences*, 10(3), 1983–2000. https://doi.org/10.5194/bg-10-1983-2013

Weiss, R. (1974). Carbon dioxide in water and seawater: The solubility of a non-ideal gas. *Marine Chemistry* https://doi.org/10.1016/0304-4203(74)90015-2, 2(3), 203–215.

Williams, N. L., Juranek, L. W., Feely, R. A., Johnson, K. S., Sarmiento, J. L., Talley, L. D., et al. (2017). Calculating surface ocean $p$$CO_2$ from biogeochemical Argo floats equipped with pH: An uncertainty analysis. *Global Biogeochemical Cycles*, 31, 1–14. https://doi.org/10.1002/2016GB005541